

Resonance chains in open systems, generalized zeta functions and clustering of the length spectrum

S. Barkhofen^{3,2}, F. Faure⁴, T. Weich^{1,2,*}

¹ Fachbereich Mathematik, Philipps-Universität Marburg,
Hans-Meerwein-Straße, 35032 Marburg, Germany

² Fachbereich Physik, Philipps-Universität Marburg, Renthof 5, 35032 Marburg,
Germany

³ Applied Physics, University of Paderborn, Warburger Strasse 100, 33098
Paderborn, Germany

⁴ Institut Fourier, 100 rue des maths, BP 74, 38402 St Martin d'Hères cedex,
France

E-mail: *: weich@mathematik.uni-marburg.de

Abstract. In many non-integrable open systems in physics and mathematics resonances have been found to be surprisingly ordered along curved lines in the complex plane. In this article we provide a unifying approach to these resonance chains by generalizing dynamical zeta functions. By means of a detailed numerical study we show that these generalized zeta functions explain the mechanism that creates the chains of quantum resonance and classical Ruelle resonances for 3-disk systems as well as geometric resonances on Schottky surfaces. We also present a direct system-intrinsic definition of the continuous lines on which the resonances are strung together as a projection of an analytic variety. Additionally, this approach shows that the existence of resonance chains is directly related to a clustering of the classical length spectrum on multiples of a base length. Finally, this link is used to construct new examples where several different structures of resonance chains coexist.

1. Introduction

The study of resonances in scattering systems with chaotic classical dynamics is an active field of research. It is at the same time driven by physicists being interested in the quantum properties of open chaotic systems as well as by mathematicians being interested in geometric analysis and partial differential equations (PDE) on non-compact manifolds. While in scattering theory, resonances are poles of the scattering matrix and correspond to quasi-stationary quantum states with purely in- or outgoing boundary conditions, from the PDE point of view resonances are often seen as the spectral invariants defined as the poles of a meromorphic continuation of the resolvent operator.

Aside from some very special exceptions (e.g. the Walsh quantized Baker map [24]) the position of the resonances of such complex systems cannot be determined exactly. It has, however, been a very successful approach to gain coarser information on general properties of the resonance distribution in terms of the underlying classical dynamics and geometry, respectively. For example results on spectral gaps [16, 25, 27] predict resonance free regions and the fractal Weyl law [33, 23, 14, 20, 32] gives an upper bound on the growth of the number of the so-called “long-living” resonances in the high frequency limit. Despite the large progress that has been made in obtaining rigorous results on the distribution of the resonances, there are still many open questions (we refer to [22] for an overview over recent results and open questions). For example the upper bound on the exponential growth of the resonance density which has been proven in the fractal Weyl law [23, 14, 33] is only conjectured to be sharp and there exists also a conjecture on the improvement of the spectral gap estimates [17]. It has thus been a very important approach to study the resonance structure numerically and by physical experiments in order to test the present conjectures and to show that the results on resonance distributions can be observed in real physical systems. There have been established two paradigmatic scattering systems for these kind of tests: the n -disk systems and Schottky surfaces.

A n -disk system describes the scattering of one particle at n -circular obstacles in the Euclidean plane (see figure 2). It has been introduced by Gaspard-Rice [12, 13, 11] and Cvitanović-Eckhardt [4] in physics and by Ikawa [16] in mathematics. In physics especially the completely symmetric 3-disk system, where 3 disks of the same size are arranged on a regular triangle, enjoys great popularity. It is already complex enough to have a classical dynamic with a non-trivial, fractal repeller and is still simple enough to be treated efficiently by numerics. There exist very efficient approaches to calculate the quantum resonances based on a direct scattering matrix ansatz [11] as well as by a semiclassical approach using zeta functions [4]. Consequently it has been among the first systems to numerically observe the fractal Weyl law [20]. Further importance arises from its experimental realizability [19] and in recent microwave experiments the spectral gap [1] and first hints of the fractal Weyl law [28] have been found. From a mathematical point of view the disadvantage of the n -disk system is that many of the numerical algorithms are not based on mathematical rigorous results. For example the conjecture that the zeros of the semiclassical zeta function are related to the quantum resonances, which has been thoroughly tested in physics [4, 40], is mathematically open (cf. [8, Section 1.6-1.8] for recent results into this direction).

This is the reason for the popularity of Schottky surfaces as an explicit model system in mathematics. Schottky surfaces are two-dimensional non-compact surfaces with constant negative curvature which are convex co-compact (see figure 7 for a

sketch of a 3-funneled Schottky surface). The constant negative curvature allows to prove that the zeros of the Selberg zeta function are related to the resonances of the Laplacian [26] and not only approximately as conjectured for the 3-disk system in physics. Furthermore Jenkinson-Pollicott [18] derived, analogously to the cycle expansion of the 3-disk system, efficient formulas to numerically compute the zeros of the Selberg zeta functions. The big drawback of these surfaces from the physical point of view is that there is no known experimental realization (see [31, 34] for attempts to realize the wave equation on negatively curved surfaces with water waves). As the curvature of these surfaces is, however, strictly negative, the geodesic flow is hyperbolic and these surfaces are an interesting model for open chaotic systems. Additionally the study of the resonances on constant negative curvature surfaces and the relation to their geometry is a mathematically interesting question itself (see e.g. [41]) thus we will call these resonances *geometric resonances*. The most simple example of Schottky surfaces which already has a non-trivial fractal repeller are the 3-funneled surfaces as shown in the upper part of figure 7. For these surfaces Borthwick recently presented a thorough numerical study of their resonances structure [3].

One of the most surprising features of this resonance structure is an observation which has before already been made for the 3-disk system [11, 40]: Even though the underlying classical dynamic is completely hyperbolic, i.e. strongly chaotic, the distribution of the resonances is highly ordered and the resonances form a striking chain structure in the complex plane (see figure 1). The 3-disk system and the Schottky surfaces are, however, not the only systems to embody these chain structures. Very similar chains have for example also been observed in higher dimensional systems, as the 4-sphere billiard [6], and even in microdisk resonators which are important models for physical applications such as microdisk lasers [39]. Furthermore the phenomenon of resonance chains is not only restricted to resonances of the Laplace operator and quantum resonances, respectively. Also the spectrum of the classical Ruelle resonances which describe the decay of correlations in classical dynamical systems has been reported to reveal these clear resonance chains [10].

Though these chains are eye-catching, little is known about these structures. For the completely symmetric 3-disk system and the completely symmetric 3-funneled Schottky surface, the distance between the resonances on one chain has been observed to be related to the length of the shortest periodic orbit [3, 40]. Additionally the oscillation length of the chains has been found to be related to the length difference between two fundamental periodic orbits. Recently a numerical study of the 3-disk system [38] showed that the resonance chains are not only a visual effect, but that the resonances on one chain share common physical properties. It was, however, shown that the resonance chains are not caused by scarring of the scattering states along individual classical orbits, but are related to the interaction of several classical orbits.

Two fundamental questions are, however, still open and will be addressed in this article. First of all the resonance chains, are a visual impression, i.e. our brain groups the resonances to different chains and we have the impression that they are strung along different continuous lines. In this article we will give a system intrinsic definition of these continuous lines. Secondly, resonance chains have been observed in many, quite different systems. We will give a unifying condition on the classical length spectrum that is able to explain and predict the existence of resonance chains.

The article is organized as follows: In Section 2 we treat the resonance chains of the symmetric 3-disk system. After a general introduction of 3-disk systems

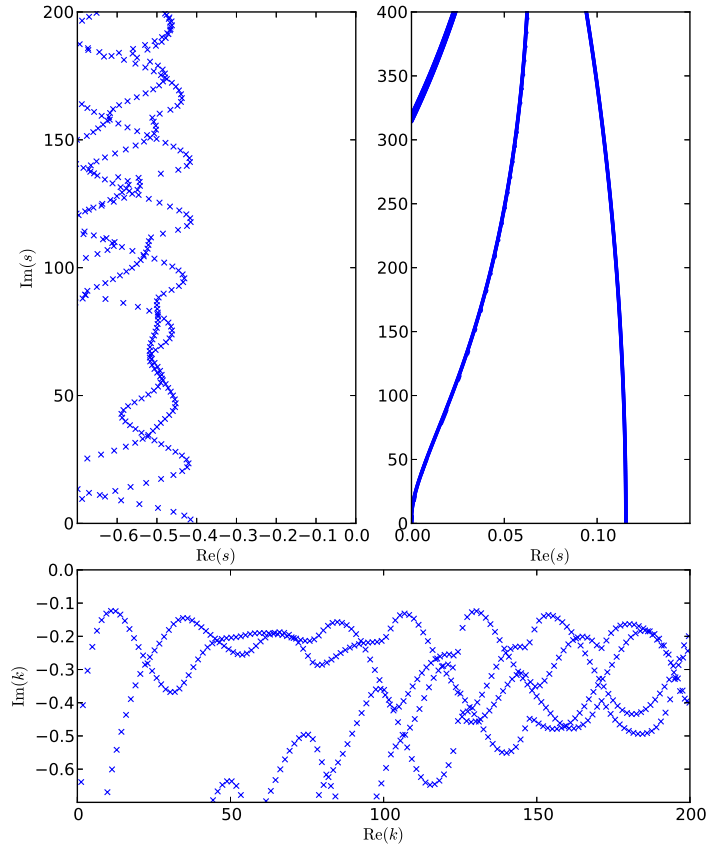


Figure 1. Resonance structure of the classical Ruelle resonances of the 3-disk system (upper left), the Schottky surface $X_{12,12,12}$ (upper right) and the quantum 3-disk system with $R/a = 6$ (lower). Note: the resonances for the Schottky surfaces are so dense that they appear as continuous lines in the plot above, however, they are discrete (see figure 8).

(Section 2.1) we will numerically illustrate that the resonance chains of the symmetric 3-disk system are created by fast rotating eigenvalues of a suitable transfer operator on the canonical Poincaré section. This idea applies for the semiclassical as well as for the classical resonances (Section 2.2). Then we give an introduction to Schottky surfaces (Section 3.1) and show in Section 3.2 that a straightforward application of this idea on the resonance spectrum of completely symmetric Schottky surfaces fails to explain the resonance chains. However, the ideas can be abstracted. This leads us to the introduction of a generalized zeta function and the generalized spectrum which are shown to be the right objects to describe and understand the resonance chains. These objects immediately also allow to deal with non-symmetric Schottky surfaces and 3-disk systems and also gives a condition for the existence of resonance chains

(Section 3.3). In Section 4 we will finally test this condition in different cases and use its predictive power to identify systems incorporating different coexistent chain structures.

As this article addresses a physical as well as a mathematical readership we decided to always state clearly which results and relations are known to be true by mathematically rigorous proofs and which results are achieved by physical arguments or experiments. This will help to keep an overview which parts of the argumentation are based on rigorous arguments and where further mathematical work remains to be done.

This article itself does not claim to derive any rigorous statements either. Instead our aim is to gain a universal understanding of the appearance of the resonance chains and to identify the mathematical quantities, which are crucial for their understanding, via numerical investigations. As the question, whether a chain structure is visible or not, is mathematically not well posed but depends on the observer of the resonance structure, our condition cannot be a *if and only if* condition either. The condition established in Section 3.2 is thus an approximate condition and our hypothesis is that the better this condition is fulfilled the clearer the chains will be visible. This hypothesis is tested and supported by various numerical results presented in Section 4. A rigorous proof of the existence of resonance will be given in [37], where the ideas and insights presented in this article are an essential ingredient.

2. 3-disk systems and rotating resonances

2.1. Introduction to 3-disk systems

A 3-disk system describes one free particle in an Euclidean 2-dimensional space that scatters at three non-overlapping hard disks D_1, D_2 and D_3 . For further use we will call the union of the disks by $D = \bigcup_i D_i$. Classically its trajectories are given by straight lines and hard wall reflections at the disk boundaries ∂D (see left panel of figure 2). Its quantum dynamics is described by the Laplacian Δ with Dirichlet boundary conditions at the disk boundaries and its quantum resonances can rigorously be defined as the poles of the resolvent

$$R(k) := (-\Delta - k^2)^{-1} : L_{\text{comp}}^2(\mathbb{R}^2 \setminus D) \rightarrow L_{\text{loc}}^2(\mathbb{R}^2 \setminus D). \quad (1)$$

This resolvent, as a map between compactly supported L^2 functions and locally L^2 -integrable functions, is known to extend meromorphically to the $\mathbb{C} \setminus l$ where l is any line connecting zero with infinity [35]. These poles do indeed coincide with the physical scattering resonances i.e. if k_n is a pole with multiplicity m , then there exist m solutions of

$$(-\Delta - k_n^2)\Psi = 0$$

with Dirichlet and purely outgoing boundary conditions. The latter condition means that the solution $\Psi(r, \phi)$ in polar coordinates (r, ϕ) can be written asymptotically in the limit $r \rightarrow \infty$ as [11]

$$\Psi(r, \phi) \sim \sum_{l=-\infty}^{\infty} C_l \frac{\exp(i(kr - l\pi/2 - \pi/4))}{\sqrt{2\pi kr}} \exp(il\phi).$$

Contrary purely incoming boundary conditions would correspond to

$$\Psi(r, \phi) \sim \sum_{l=-\infty}^{\infty} C_l \frac{\exp(-i(kr - l\pi/2 - \pi/4))}{\sqrt{2\pi kr}} \exp(il\phi).$$

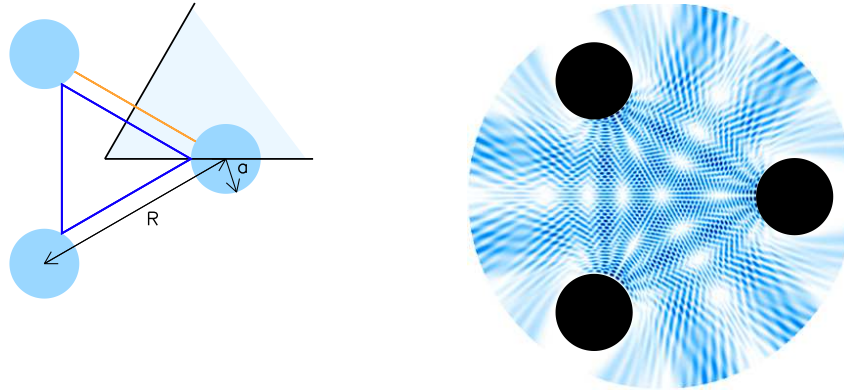


Figure 2. Left: Sketch of a symmetric 3-disk system and two classical closed trajectories (yellow and blue lines). The fundamental domain is shaded in light blue. The symmetry reduced billiard is then a billiard consisting of the fundamental domain with two additional hard walls along the symmetry axes. Right: Quantum mechanical scattering state with Dirichlet boundary conditions and purely outgoing boundary conditions calculated by the algorithm as described in [38]. Note that this scattering state is additionally vanishing along the symmetry axes and is thus also a scattering state of the symmetry reduced billiard with Dirichlet boundary conditions.

Here C_l are constant coefficients and for fixed l the asymptotic r, ϕ dependence equals the asymptotic dependence of a free particle state with angular momentum l .

An important class of 3-disk systems are those which are completely symmetric. In those systems all three disks have the same size and the disks are arranged on an equilateral triangle (see left part of figure 2). Historically the side length of the triangle is denoted by R and the disk radius by a [13]. These systems are then completely characterized, up to a scaling, by the ratio R/a . As the system is highly symmetric and possesses the symmetry group D_3 of the equilateral triangle often the symmetry reduced system is studied in physics. This system consists of an open billiard representing the fundamental domain of the 3-disk system (see light shaded region in the left part of figure 2).

As already mentioned before the classical time evolution of a particle between two disk reflections is just a linear propagation interspersed with hard wall reflections. The trajectory of a particle therefore does not depend on the absolute value of its momentum and we can always scale it to 1. It is furthermore convenient to get rid of the parts of linear propagation where no complex dynamic takes place and consider only the Poincaré section of disk reflections. A particle at the boundary of a disk D_i of radius a_i whose momentum is scaled to one, is completely described by its Birkhoff coordinates (q, p) . They are defined as the arc length $q \in [-\pi a_i, \pi a_i]$ on the disk boundary as well as the projection of the normalized incoming momentum to the unit tangent vector at the disk boundary $p = \vec{p} \cdot \vec{t} = \cos(\alpha) \in [-1, 1]$ (see figure 3). The complete space \mathcal{P} of the Poincaré section consists of three copies of $[-\pi a_i, \pi a_i] \times [-1, 1]$. As the system is open the dynamics are not defined on all \mathcal{P} , because in many cases a particle with Birkhoff coordinates (q, p) will just escape to infinity after the reflection and will not hit any of the other disks in the future. We therefore introduce the forward trapped set $\mathcal{T}_+^{(n)}$ of order n as the set of all points in

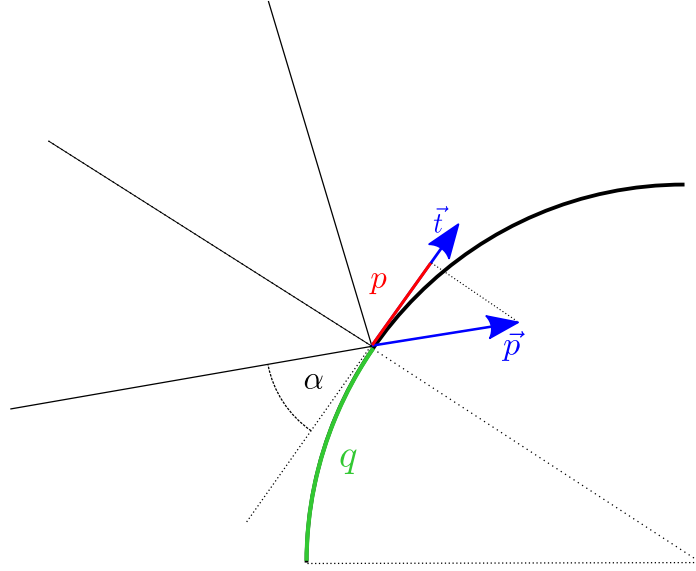


Figure 3. Sketch illustrating the Birkhoff coordinates. The Birkhoff coordinates of a trajectory being reflected at the disk boundaries are given by the position of the reflection on the boundary, measured by the arc length of the impact point with respect to a fixed reference point (denoted by q in the figure) and by the projection of the unit momentum vector on the unit tangent vector.

\mathcal{P} which will hit at least n disks on their future trajectories. Analogously we define the backward trapped set $\mathcal{T}_-^{(n)}$ for the time inverted dynamics. The discrete time dynamics on the Poincaré section is then a diffeomorphism

$$\phi : \mathcal{T}_+^{(1)} \rightarrow \mathcal{T}_-^{(1)}.$$

Note that this diffeomorphism only leaves invariant the trapped set

$$\mathcal{T} = \bigcap_{n=1}^{\infty} \mathcal{T}_+^{(n)} \cap \mathcal{T}_-^{(n)}$$

which is known to be a fractal subset of \mathcal{P} if the 3 disks are sufficiently far away from each other [12]. Using this discrete time dynamics we can define for any smooth function $V : \mathcal{T}_+^{(1)} \rightarrow \mathbb{C}$ the transfer operator $\mathcal{L}_V : C_0^\infty(\mathcal{T}_+^{(1)}) \rightarrow C^\infty(\mathcal{P})$ by setting

$$(\mathcal{L}_V f)(x) = V(\phi^{-1}(x))f(\phi^{-1}(x))$$

which is an operator with integration kernel

$$K(x, y) = V(y)\delta(\phi^{-1}(x) - y). \quad (2)$$

In the theory of dynamical systems this function V is commonly called the *potential function* even if V does not at all play the role of a potential in the sense of classical mechanics. With this transfer operator we can now introduce the zeta function. If we suppose that \mathcal{L}_V can be extended to a Banach space \mathcal{B} such that \mathcal{L}_V is trace class

then we can study the dynamical zeta function associated to the potential V which is defined by the Fredholm determinant[‡]

$$d_{\text{Fred}}(z) := \det(1 - z\mathcal{L}_V) = \exp\left(-\sum_{n>0} \frac{z^n}{n} \text{Tr}(\mathcal{L}_V^n)\right). \quad (3)$$

This function is then known to be analytic in z and the discrete spectrum $\sigma(\mathcal{L}_V)$ of the transfer operator is related to the zeros of the dynamical zeta function by

$$\sigma(\mathcal{L}_V) = \{z \setminus \{0\} \in \mathbb{C}, d_{\text{Fred}}(1/z) = 0\}.$$

By the explicit form (2) of the kernel $K(x, y)$ we can on the other hand formally define the so-called flat trace

$$\text{Tr}^b(\mathcal{L}_V^n) := \sum_{x \in \text{Fix}(\phi^n)} \frac{V_n(x)}{|\det(1 - (D\phi^n)(x))|},$$

where $(D\phi^n)(x) \in \mathbb{R}^{2 \times 2}$ is the Jacobian of ϕ^n , $V_n(x) = \prod_{k=1}^n V(\phi^k(x))$ the iterated product and $\text{Fix}(\phi^n)$ the set of all fixed points of ϕ^n . By the flat trace we can define in complete analogy to (3) another zeta function by

$$d^b(z) := \exp\left(-\sum_{n>0} \frac{z^n}{n} \sum_{x \in \text{Fix}(\phi^n)} \frac{V_n(x)}{|\det(1 - (D\phi^n)(x))|}\right). \quad (4)$$

By a standard calculation for zeta functions (see Appendix A) this expression can be brought to the form

$$d^b(z) := \prod_{p \in P} \prod_{k=0}^{\infty} \left(1 - z^{n_p} \frac{V_p}{|\Lambda_p| \Lambda_p^k}\right)^{k+1}. \quad (5)$$

Here P is the set of all *primitive periodic orbits* of the map ϕ , i.e. the set of all periodic orbits $\{x, \phi(x), \dots, \phi^m(x) = x\}$ for which there is no $1 < k < m$ which also fulfills $\phi^k(x) = x$. Furthermore n_p is the discrete time length of this orbit, V_p is the iterated product of the potential V along the primitive orbit p and Λ_p is the eigenvalue of $D\phi^{n_p}(x_p)$ whose absolute value is larger than one.

It is important to note that the expressions (4) and (5) only converge absolutely for $|z|$ sufficiently small. Furthermore (4) directly implies that the zeta function has no zeros in the region of absolute convergence. Equations (4) and (5) are thus of no direct use for a calculation of the zeros of the dynamical zeta function. If one knows, however, that $d^b(z)$ can be extended analytically beyond the region of absolute convergence, its Taylor expansion in z around zero

$$d^b(z) = \sum_{n=0}^{\infty} C_n z^n$$

will automatically converge absolutely on any disk contained in the region of analytic continuation. This trick has been introduced in physics by Cvitanović and Eckhardt [4] under the name cycle expansion.

From a mathematical point of view, the biggest challenge is to prove the analytic continuation of the zeta function defined by (4) and to show that its zeros correspond to the spectrum of \mathcal{L}_V . This is for example possible if one finds function spaces such

[‡] To our knowledge such a function space is not known. In physics literature such an assumption is, however, often implicitly made.

that \mathcal{L}_V is trace class and that its trace in this space equals the flat trace. Then one obtains by the analyticity of the Fredholm determinant automatically an analytic continuation of the zeta function. Such results are known for several classes of systems (for example for real analytic expanding or hyperbolic maps [29, 30, 7]) but to our knowledge not in any setting in which the 3-disk system fits.

Physicists usually skip this difficulty and test for concrete examples in which regions the cycle expansion numerically converges. It is then assumed that this region coincides with the region of analytic continuation. Furthermore it is usually assumed that the zeros of the zeta function defined by the flat trace (4) are eigenvalues of the transfer operator. As there is not yet a satisfying mathematical theory in the case of the 3-disk system we will also make these assumptions from now on.

For the 3-disk system two particular choices for the potential are of special interest as they lead to the classical zeta function and to the semiclassical or Gutzwiller-Voros zeta function, respectively. The return time or return length of a particle at the disk boundary with Birkhoff coordinates $x \in \mathcal{T}_+^{(1)}$ is defined as the length of the trajectory until the next disk reflection. This defines a smooth bounded function

$$\tau : \mathcal{T}_+^{(1)} \rightarrow \mathbb{R}^+$$

and we first can consider for $s \in \mathbb{C}$ the analytic family of potentials

$$V_s^{cl}(x) = e^{-s\tau(x)}. \quad (6)$$

Plugging this potential into (5) we obtain a dynamical zeta function depending on two variables s, z

$$d^{cl}(s, z) := \prod_{p \in P} \prod_{k=0}^{\infty} \left(1 - z^{n_p} \frac{e^{-s\tau_p}}{|\Lambda_p| \Lambda_p^k} \right)^{k+1},$$

where τ_p is the Birkhoff sum along this orbit defined by

$$\tau_p = \sum_{k=1}^{n_p} \tau(\phi^k(x))$$

for x being an arbitrary point on the orbit p . It is related to the Selberg-Smale zeta function by [10]

$$Z(s) = d^{cl}(s, 1).$$

This zeta function is of special interest because its zeros, the so-called Ruelle resonances, determine the decay of correlations of the classical dynamical system (at least for systems where the theory of Ruelle resonances is established, for the 3-disk system this is again conjectured to be true, c.f. [10]). This is why these zeta functions have been studied numerically by Gaspard and Ramirez [10] for the symmetric 3-disk system where they observed the resonance chains presented in figure 1.

Using the ideas of [9] we can also express the Gutzwiller-Voros zeta function by transfer operators. We therefore define the function $\Lambda(x)$ on $\mathcal{T}_+^{(1)}$ to be the restriction of the Jacobian $D\phi(x)$ to the unstable direction which is simply given by the multiplication with a nonzero number. If x is a fixed point of an iteration of the Poincaré map $\phi^n(x) = x$, then the iterated product of $\Lambda(x)$ will be exactly the unstable eigenvalue Λ_n of $D\phi^n$.

With this function we define

$$V_s^{(a)}(x) = -|\Lambda(x)|^{1/2} e^{-s\tau(x)} \text{ and } V_s^{(b)}(x) = |\Lambda(x)|^{-1/2} e^{-s\tau(x)}$$

as well as the corresponding Fredholm determinants

$$d^{(a)}(s, z) = \det(1 - z\mathcal{L}_{V_s^{(a)}}) \text{ and } d^{(b)}(s, z) = \det(1 - z\mathcal{L}_{V_s^{(b)}}).$$

We can then study the quotient

$$\begin{aligned} \frac{d^{(a)}(s, z)}{d^{(b)}(s, z)} &= \exp \left(- \sum_{n>0} \frac{z^n}{n} \sum_{x \in \text{Fix}(\phi^n)} \frac{e^{-s\tau_n(x) - in\pi} (|\Lambda_n(x)|^{1/2} - (-1)^n |\Lambda_n(x)|^{-1/2})}{|\det(1 - (D\phi^n)(x))|} \right) \\ &= \exp \left(- \sum_{n>0} \frac{z^n}{n} \sum_{x \in \text{Fix}(\phi^n)} \frac{e^{-s\tau_n(x) - in\pi}}{\sqrt{|\det(1 - (D\phi^n)(x))|}} \right). \end{aligned}$$

For the last equality we used that the Poincaré map is orientation inverting and consequently $\Lambda(x) < 0$ which implies that

$$\sqrt{|\det(1 - (D\phi^n)(x))|} = |\Lambda_n(x)|^{1/2} - (-1)^n |\Lambda_n(x)|^{-1/2}.$$

The final expression is related to the so-called Gutzwiller-Voros zeta function [36] by

$$Z_{GV}(k) = \frac{d^{(a)}(-ik, 1)}{d^{(b)}(-ik, 1)}. \quad (7)$$

It has been numerically thoroughly checked [4, 40] that the zeros of $Z_{GV}(k)$ coincide to a high precision to the quantum resonance which have numerically been obtained by a quantum scattering approach. It is conjectured that the zeros of the Gutzwiller-Voros zeta function converge towards the quantum resonances in the semiclassical limit. This relation [13] is, however, based on the Gutzwiller-trace formula for the quantum propagator beyond the Ehrenfest time, and from the mathematical point of view the relation to the quantum spectrum is completely open §. For practical purpose this relation between the zeros of the zeta function and the quantum resonances has, however, a huge advantage because especially in the regime of high energies the calculations of the zeros of $Z_{GV}(k)$ via the cycle expansion is much faster than the calculation based on the quantum scattering matrix and it has been exploited in many numerical works on the quantum spectrum [20, 6, 39].

2.2. Rotating resonances

We now want to understand the resonance chains for the symmetric 3-disk system via the zeta functions introduced above. The zeta functions allow to handle the resonance chains for classical Ruelle resonances and quantum resonances by the same approach, even though the physical nature of these resonances is completely different.

In both cases one has a zeta function $Z(s, z)$ which depends on two complex variables and the resonances are defined by ||

$$\text{Res} = \{s \in \mathbb{C}, Z(s, 1) = 0\}.$$

Note that for the quantum case we use the hypothesis that the semiclassical and quantum resonances coincide. We will, however, only use this correspondence for the

§ For closed systems there has recently been derived a relation between the quantum and the so-called prequantum operator which is an important step into this direction [8].

|| In the case of quantum resonances the resonance set is usually the set $\text{Res} = \{k \in \mathbb{C}, Z(-ik, 1) = 0\}$ (see (7)). In order to emphasize the uniform approach to quantum and classical resonances as well as the geometric resonances on Schottky surfaces, we will, however, from now on consider the quantum resonances to be parametrized by $s = -ik$ which simply leads to a clockwise rotation by 90° of the quantum resonances in the plots.

symmetric 3-disk system in an energy regime, where this correspondence is known to hold with a very high precision [4, 40]. Beside the set of resonances which we have defined to be the zeros in s of $Z(s, z)$ for fixed $z = 1$ it seems also natural to consider for a fixed $s \in \mathbb{C}$ the zero set in z . In order to have a direct physical interpretation of this set we consider the inverses of these zeros and define for a fixed $s \in \mathbb{C}$

$$\sigma_s := \{z \in \mathbb{C} \setminus \{0\}, Z(s, 1/z) = 0\}. \quad (8)$$

Using the Fredholm determinant representation of the classical zeta function

$$Z_{cl}(s, z) = \det(1 - z\mathcal{L}_{V_s^{cl}})$$

one directly identifies $\sigma_s = \sigma(\mathcal{L}_{V_s^{cl}})$ which is the spectrum of $\mathcal{L}_{V_s^{cl}}$. For the semiclassical resonances this identification is slightly more subtle as Z_{GV} has been defined as the quotient of two zeta functions. If we assume, however, that $d^{(b)}(s, z)$ is analytic in a neighborhood of $z \in \sigma_s$, then the Gutzwiller-Voros zeta function can only vanish if the nominator of the quotient vanishes, i.e. if

$$0 = d^{(a)}(s, z^{-1}) = \det(1 - z^{-1}\mathcal{L}_{V_s^{(a)}})$$

and $z \in \sigma(\mathcal{L}_{V_s^{(a)}})$. Note that the analyticity assumption of $d^{(b)}(s, z)$ is not very strong and in the s -range which we will consider in the sequel it is always fulfilled (see Appendix C)

Summarizing, we have the following two objects in the classical as well as in the semiclassical or quantum case: On the one hand we have the resonance spectrum which equals the zeros of the zeta function in s for $z = 1$ and on the other hand we have for any $s \in \mathbb{C}$ the discrete set σ_s which can be interpreted as the eigenvalues of a transfer operator \mathcal{L}_s which is parametrized by a complex number s . Obviously s is a resonance if and only if the operator \mathcal{L}_s has 1 as an eigenvalue i.e.

$$s \in \text{Res} \Leftrightarrow 1 \in \sigma_s.$$

The simple but important observation is now the following: If we start with a resonance $s_0 \in \text{Res}$ of multiplicity one and continuously vary the parameter s then we will be able to trace the eigenvalue which was equal to 1 for $s = s_0$ and which continuously depends on s . We will call this eigenvalue $\lambda_{s_0}(s)$. A closer look in the concrete form of our transfer operators \mathcal{L}_s allows us to predict how the eigenvalues will approximately depend on s . In the quantum case for $\mathcal{L}_s = \mathcal{L}_{V_s^{(a)}}$ as well as in the classical case with $\mathcal{L}_s = \mathcal{L}_{V_s^{cl}}$ we have

$$\mathcal{L}_s = \mathcal{L}_0 e^{-s\tau(x)}$$

where $e^{-s\tau(x)}$ is simply the multiplication operator. In the case of the symmetric 3-disk system the return time is a smooth function which becomes more and more homogeneous the bigger R/a becomes. Assuming as a first order approximation that $\tau(x) \approx \tau_0 = R - 2a$ then

$$\lambda_{s_0}(s) = e^{-s\tau_0}.$$

If this approximation was exactly true and if we moved with s parallel to the imaginary axis, then the eigenvalue $\lambda_{s_0}(s)$ would simply rotate around zero on the unit circle. Note that by the definition of the resonance set, every s value for which $\lambda_{s_0}(s)$ crosses the value point 1 on the unit circle is itself a resonance. By this argument a single eigenvalue of \mathcal{L}_{s_0} would create a whole chain of resonances, parallel to the imaginary axis. The resonances would be equally distributed along this chain with a distance of $2\pi/\tau_0$. As the return time is in reality not exactly constant one would expect that

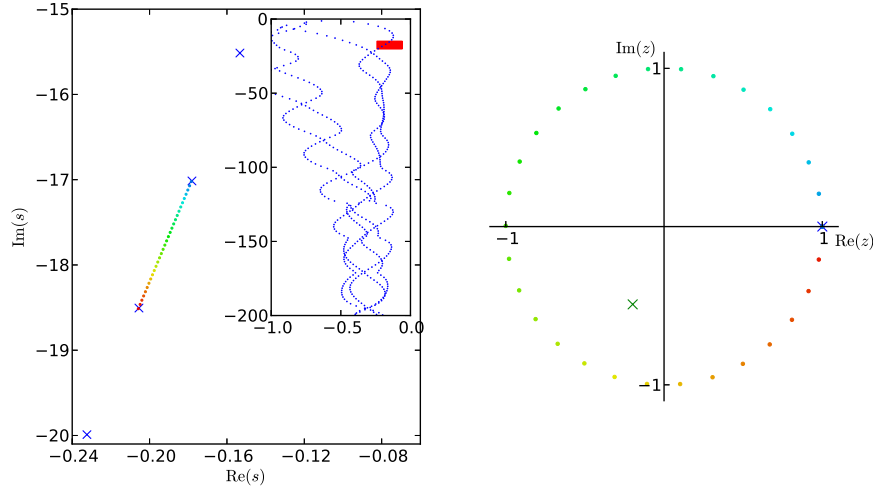


Figure 4. Left: Plot of the quantum resonances of the 3-disk system with $R/a = 6$. The inset shows the chain structure of the resonances on a large domain in the complex plane. The main plot shows a strong zoom into one chain, such that only few individual resonances are in the plot region (blue crosses). The region of the zoom is indicated in the inset by a red rectangle. The colored dots between the two resonances $s_1 = -0.206 - 18.51i$ and $s_2 = -0.178 - 17.02i$ represent a discrete interpolation between the two resonances. The interpolation follows the line suggested by the resonance chains. Right: Spectrum of the transfer operator on the Poincaré section. The blue crosses represent the spectrum of \mathcal{L}_{s_1} with $|z| > 0.3$. By the colored dots we follow the evolution of the eigenvalue starting at 1 for s_1 while s varies as indicated by the colored points in the left panel. The evolution of the second eigenvalue is not plotted for more clarity.

slight variations deform the chains and also lead to a distance variation between the extremal values of the return time.

It can be checked numerically that it is exactly this mechanism of a rotating eigenvalue of the operator \mathcal{L}_s which creates the resonance chains. In figure 4 this is visualized for the quantum resonances of the symmetric 3-disk system with $R/a = 6$. On the left we can see a plot of the quantum resonances s_n in the complex plane[¶]. On the right the spectrum of the transfer operator $\mathcal{L}_{V_s^{(a)}}$ is presented. The blue crosses indicate the eigenvalues with $|z| > 0.3$ for an s -value which equals the resonance $s_1 = -0.206 - 18.51i$. As expected we find an eigenvalue which is equal to 1. There is also another eigenvalue plotted which corresponds to the second chain which is nearby the chain to which s_1 belongs. There are further eigenvalues of the transfer operator near zero which we did not plot as the convergence of the zeta function becomes more and more complicated the smaller the absolute values of z . The colored points show how the eigenvalue at 1 moves, if the s values varies between two resonances s_1 and $s_2 = -0.178 - 17.02i$. As suggested by the heuristic arguments above the eigenvalue moves along the unit circle in a clockwise orientation and creates the next resonances on the chain. Exactly the same can be observed for the classical Ruelle resonances of the 3-disk system with $R/a = 6$ (see figure 5).

[¶] Note that as discussed above the usual parametrization of quantum resonances is $k_n = is_n$.

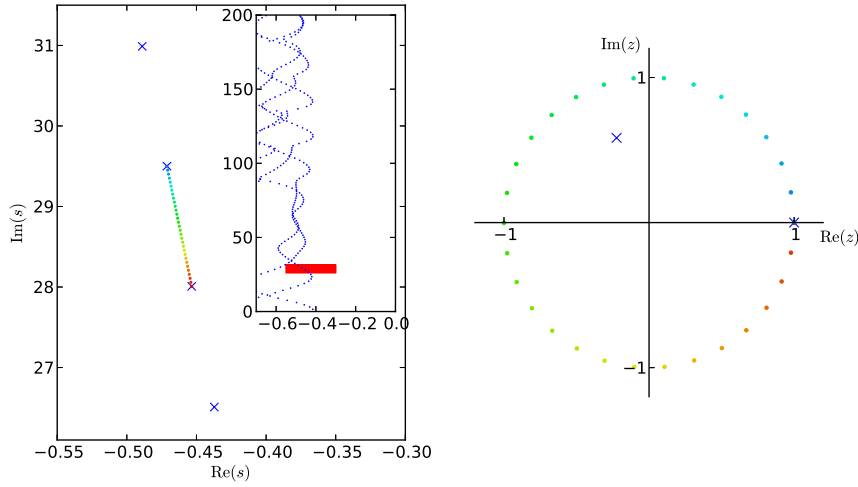


Figure 5. Left: Plot of the classical Ruelle resonances of the 3-disk system with $R/a = 6$. The inset shows the chain structure of the resonances on a large domain in the complex plane. The main plot shows a strong zoom into one chain, such that only few individual resonances are in the plot region (blue crosses). The region of the zoom is indicated in the inset by a red rectangle. The colored dots between the two resonances $s_1 = 0.453 + 28.0i$ and $s_2 = 0.471 + 29.5i$ represent a discrete interpolation between the two resonances following the line suggested by the resonance chains. Right: Spectrum of the transfer operator on the Poincaré section. The blue crosses represent the spectrum of \mathcal{L}_{s_1} with $|z| > 0.3$. By the colored dots we follow the evolution of the eigenvalue starting at 1 for s_1 .

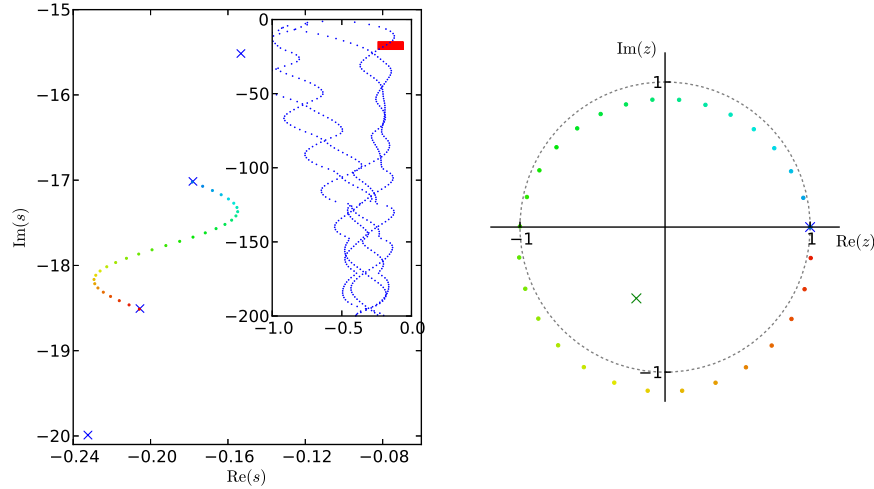


Figure 6. Same as in figure 4. However the colored dots between the two resonances $s_1 = -0.206 - 18.51i$ and $s_2 = -0.178 - 17.02i$ now do not follow the line which is suggested by the resonance chains but a deformed path. As a consequence the eigenvalue of \mathcal{L}_{s_1} starting at 1 for s_1 now turns one time around zero on a path which is not on the unit circle (black,dotted).

These numerical results do, however, not only confirm that the hypothesis that each resonance chain is created by a rotating \mathcal{L}_s -eigenvalue is true. They also indicate what the continuous mathematical object is that the resonances are distributed on. Note that taking two neighboring resonances of one chain there are multiple paths to connect these two resonances. While each path will effectively lead to one rotation of $\lambda_{s_0}(s)$ around zero, there is only one such path, for which $\lambda_{s_0}(s)$ stays on the unit circle. As it can be seen in figure 4 such a rotation on the unit circle is obtained if the two resonances are connected along the path which is suggested by the structure of the resonance chains. If one, however, takes a different path between the two resonances, then the corresponding eigenvalue of \mathcal{L}_s will turn on a deformed circle around zero (see figure 6 for an arbitrary path between the two resonances). We can thus define

$$\mathcal{C} := \{(s, z) \in \mathbb{C}^2, Z(s, z) = 0, |z| = 1\} \subset \mathbb{C}^2$$

and from the numerics above we conclude that the continuous object on which the resonances are distributed is given by $\text{Pr}_s(\mathcal{C})$ where $\text{Pr}_s : \mathbb{C}^2 \rightarrow \mathbb{C}$ is the projection on the s -component.

We have thus seen in this section that the resonance chains of the classical and the quantum resonances are generated by the same mechanism. As in both cases the resonances can be seen as the zero set in s of a zeta function, which can be represented as a Fredholm determinant of a s -dependent family of operators. The resonance chains are generated by single eigenvalues of \mathcal{L}_s which circle around zero while s moves along the chain. Furthermore this approach allows a system-intrinsic definition of a continuous object that coincides with the visually suggested curves on which the resonances are strung together. In the next section we will see how this idea can be extended to the resonance chains on Schottky surfaces and examine in detail the question in which systems resonance chains will occur and in which not.

3. Schottky surfaces and generalized zeta functions

3.1. Introduction to Schottky surfaces

Schottky surfaces are a special class of infinite volume Riemann surfaces. In this section we will give a brief introduction to its most important properties. For a detailed introduction we refer to [2].

The easiest way to define Schottky surfaces is as a quotient of the upper half plane by a so-called Schottky group. The upper half plane $\mathbb{H} = \{u = x + iy \in \mathbb{C}, y > 0\}$ together with the Riemannian metric $(dx^2 + dy^2)/y^2$ has a constant negative Gauss curvature $\kappa = -1$ and is a standard model of hyperbolic geometry. The group $SL(2, \mathbb{R})$ of real invertible matrices with determinant one acts on \mathbb{H} via Moebius transformations

$$\begin{pmatrix} a & b \\ c & d \end{pmatrix} u := \frac{au + b}{cu + d}. \quad (9)$$

In fact for every $A \in SL(2, \mathbb{R})$ the Moebius transformation is an orientation preserving isometry and all orientation preserving isometries of the upper half-plane can be expressed as an $SL(2, \mathbb{R})$ -action. A Schottky group is then a discrete subgroup $\Gamma \subset SL(2, \mathbb{R})$ which is constructed in the following way: Let D_1, \dots, D_{2r} be disks with centers on the real line and mutually disjoint closure. Then for every $1 \leq i \leq r$ there exists an element $S_i \in SL(2, \mathbb{R})$ that maps the boundary ∂D_i to the boundary

of ∂D_{i+r} and the interior of D_i to the exterior of D_{i+r} . From the disjointness of the disks follows that the elements S_1, \dots, S_r are the generators of a free discrete subgroup

$$\Gamma = \langle S_1, \dots, S_r \rangle \subset SL(2, \mathbb{R})$$

and such groups are called *Schottky groups*. The quotient

$$X = \Gamma \backslash \mathbb{H}$$

is then again a surface with constant negative curvature and is called *Schottky surface*.

The 3-funneled surfaces, which we are interested in, are from the dynamical point of view the simplest nontrivial example and they are constructed from four disks arranged as in figure 7. The surface can be thought as the set $\mathbb{H} \setminus \cup D_i$ glued together along the two dotted blue half circles as well as along the two dashed red half circles (see figure 7). It is known that such 3-funneled Schottky surfaces are uniquely determined by the three lengths l_1, l_2, l_3 of the geodesics $\gamma_1, \gamma_2, \gamma_3$ that wind once around one of the 3-funnels (see upper part of figure 7). Furthermore for any triple of positive numbers l_1, l_2, l_3 there exists a 3-funneled Schottky surface which has fundamental geodesics of this length and we will call this surface X_{l_1, l_2, l_3} .

In order to define the geometric resonances on a Schottky surface X we consider the positive Laplacian which is defined by the metric and which we call Δ_X and we define the resolvent

$$R_X(s) := (\Delta_X - s(s-1))^{-1}.$$

By Mazzeo-Melrose [21] and Guillope-Zworski [15] we know that the resolvent admits a meromorphic continuation and we define the resonance set Res_X again as the set of its poles. Note that the resolvent's parametrization is different from the parametrization via k in the 3-disk case, which leads to the fact that the resonance chains do not oscillate along the real axis but along the imaginary axis. This parametrization is, however, very useful as it admits the following exact relation between the resonances of the Laplacian and a zeta function:

Let P_X be the set of all primitive closed geodesics on X , i.e. those closed geodesics that cannot be obtained by repeating a shorter closed geodesic. If for $\gamma \in P_X$, $l(\gamma)$ denotes the length of the periodic geodesic, then the Selberg zeta function is defined as

$$Z_X(s) = \prod_{\gamma \in P_X} \prod_{m=0}^{\infty} \left(1 - e^{-(s+m)l(\gamma)}\right). \quad (10)$$

This product is known to converge uniformly on any compact set with $\text{Re}(s) > 1$ and for X being a Schottky surface the Selberg zeta function is known to extend analytically to the whole complex plane \mathbb{C} and there is the following relation between its zeros and the resonances of Δ_X : If $Z_X(s) = 0$ then s is either a topological zero with $s = 0, -1, -2, \dots$ or a resonance i.e. $s \in \text{Res}_X$ [26].

For Schottky surfaces we can express the Selberg zeta function as a Fredholm determinant of a transfer operator. We therefore define the *Bowen-Series map* of a Schottky group $\Gamma = \langle S_1, \dots, S_r \rangle$ by

$$B : \begin{cases} \bigcup_{i=1}^{2r} D_i & \rightarrow & \mathbb{C} \\ u & \mapsto & S_i u \text{ if } u \in D_i. \end{cases}$$

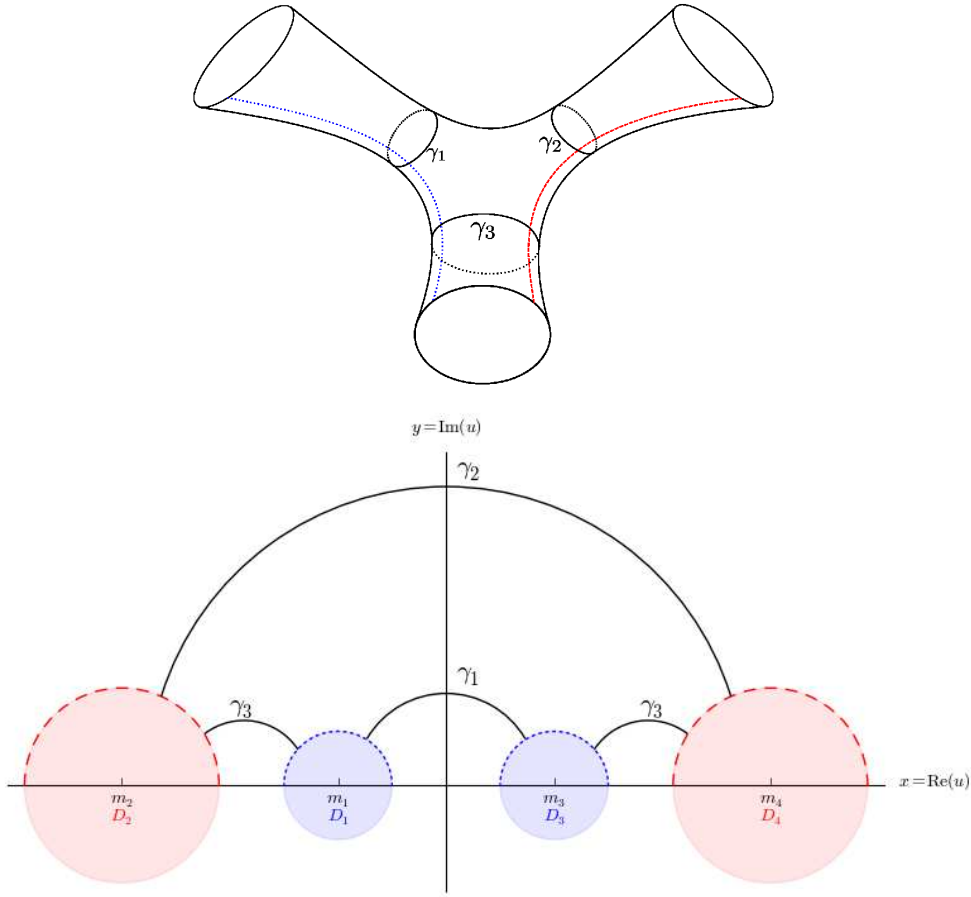


Figure 7. Upper part: Sketch of a Schottky surface with three funnels and the three fundamental closed geodesics $\gamma_1, \gamma_2, \gamma_3$. The dotted blue and dashed red lines indicate the lines along which the fundamental domain is glued together in order to obtain the surfaces. Lower part: Configuration of 4 disks that give rise to the construction of the Schottky group for a 3-funneled surface. The upper half plane without the disks represents a fundamental domain and the surface can be obtained by gluing together the red dashed lines with the blue dotted lines. In black the three fundamental closed geodesics $\gamma_1, \gamma_2, \gamma_3$ from the upper part of the figure are shown. While γ_1 and γ_2 are only represented by one arc each, the geodesic γ_3 appears as two arcs in the fundamental domain.

Here we used the convention that for $r < i \leq 2r$, $S_i := S_{i-r}^{-1}$. We can then define a family of transfer operators parametrized by $s \in \mathbb{C}$ via its action

$$(\mathcal{L}_s f)(u) := \sum_{v \in B^{-1}(u)} B'(v)^{-s} f(v),$$

where B' is the complex derivative of the Bowen-Series map and $u \in \cup_i D_i$. These transfer operators are known to be trace class on the space of holomorphic L^2 -functions on $\cup_i D_i$ (see [29] for the original proof in slightly different functions spaces or [2, Lemma 15.6]) and one therefore knows that its dynamical zeta function

$$d_{BS}(s, z) := \det(1 - z\mathcal{L}_s)$$

is analytic. We will give a short sketch of the idea how to relate the dynamical zeta function to the Selberg zeta function. For more details we refer to [2, Section 15.3]. One first can prove that the trace of \mathcal{L}_s equals its flat trace and obtains

$$d_{BS}(s, z) = \exp \left(- \sum_{n>0} \frac{z^n}{n} \sum_{u \in \text{Fix}(B^n)} \frac{(B^n)'(u)^{-s}}{|1 - (B^{-n})'(u)|} \right). \quad (11)$$

As in the case of the 3-disk system (cf. equation (5) and Appendix A) one can transform the dynamical zeta function into a product over prime orbits of the Bowen-Series map B . In a second step one can prove that the set of primitive periodic geodesics is in one-to-one correspondence to the primitive periodic orbits of the Bowen-Series maps, i.e. for each $\gamma \in P_X$ there exists a unique $n \in \mathbb{N}$ and a periodic orbit $\{u, B(u), \dots, B^n(u) = u\}$ and the length of the geodesic is related to the stability of the fixed point by

$$e^{l(\gamma)} = (B^n)'(u).$$

If we denote this n as the *Bowen-Series order* $n_{BS}(\gamma)$ of the geodesic γ , then we obtain, combining all arguments

$$d_{BS}(s, z) = \prod_{\gamma \in P_X} \prod_{m=0}^{\infty} \left(1 - z^{n_{BS}(\gamma)} e^{-(s+m)l(\gamma)} \right). \quad (12)$$

In particular this yields $d_{BS}(s, 1) = Z_X(s)$ and we deduce that $s \in \text{Res}_X$ implies that \mathcal{L}_s has an eigenvalue equal to 1.

3.2. Generalized zeta function and spectra

The previous discussion on the relation between the spectrum of \mathcal{L}_s and the resonances of the Laplacian, together with the observations from Section 2.2 that for 3-disk systems rotating eigenvalues of a transfer operator create the resonance chains would suggest that the resonance chains for the 3-funneled Schottky surfaces are generated by rotating eigenvalues of the Bowen-Series transfer operator \mathcal{L}_s . However, this idea fails completely to explain the resonance chains for the 3-funneled symmetric surfaces: In figure 8 we have plotted for $X_{12,12,12}$ the spectrum of \mathcal{L}_s for different s -values interpolating between two resonances s_1 and s_2 . We observe that the eigenvalues start to turn while we move along the chain. However, the eigenvalue which was equal to 1 for $s = s_1$ is drawn towards zero and when we approach $s = s_2$ it is another eigenvalue of \mathcal{L}_s which has been coming out from the interior, that creates the next resonance. In order to understand why a direct application of the idea of rotating eigenvalues to the spectrum of the Bowen-Series transfer operator \mathcal{L}_s fails, we recall that for the 3-disk system it has been an important argument that the return time of the Poincaré section is very homogeneous. This assumption is, however, not at all fulfilled for the standard Bowen-Series map, which corresponds morally to a Poincaré section⁺ indicated by the blue and red lines in figure 7. The return time or return length respectively is thus very inhomogeneous: While on $X_{12,12,12}$ for the closed geodesics γ_1 and γ_2 the return length is equal to 12, it equals only 6 for the geodesic γ_3 as this geodesic crosses the Poincaré section twice.

⁺ To be more precise, a Poincaré section along these two lines would be a bijective hyperbolic map on a two dimensional space. The Bowen-Series map can then be obtained as the restriction of this Poincaré map to the instable direction, which makes it expanding but not invertible anymore.

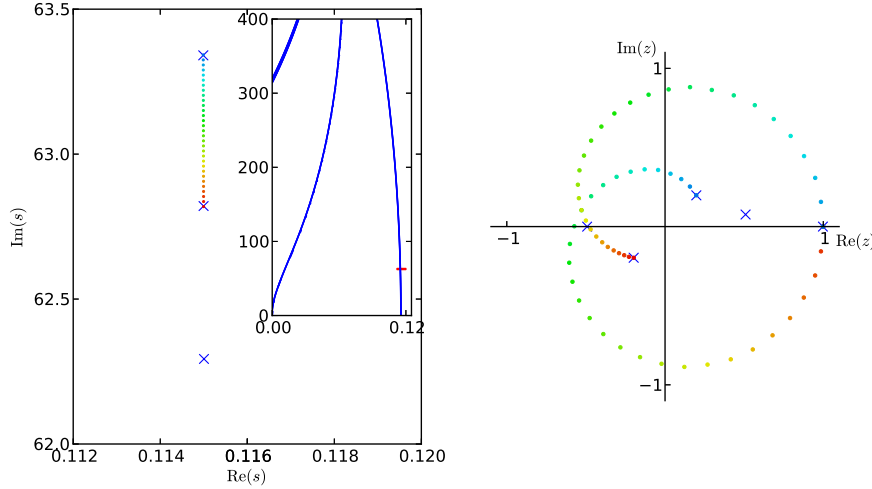


Figure 8. Left: Plot of the resonances of $X_{12,12,12}$. The inset shows the chain structure of the resonances on a large domain in the complex plane. The main plot shows a strong zoom into one chain, such that the individual resonances become visible (blue crosses). The region of the zoom is indicated in the inset by a red rectangle. The colored dots between the two resonances $s_1 = 0.1150 + 62.82i$ and $s_2 = 0.1150 + 63.34i$ represent a discrete interpolation between the two resonances, following the line suggested by the resonance chains. Right: Spectrum of the Bowen-Series transfer operator with $|z| > 0.2$. The blue crosses represent the spectrum of \mathcal{L}_{s_1} . By the colored dots we follow the evolution of two particular eigenvalues, as the s -values evolve as indicated by the colored points in the left panel. We only follow the evolution of the eigenvalue starting at 1 for s_1 and the one ending at 1 for s_2 . The evolution of the other eigenvalues is not shown for more clarity.

In order to fix this issue we could try to construct another transfer operator which still has the property that its dynamical zeta function is related to the Selberg Zeta function but which has a homogeneous return time for the completely symmetric 3-funneled Schottky surface. Such a construction is in principle possible (see [37]), this solution would then, however, be restricted to completely symmetric Schottky surfaces. Non-symmetric surfaces, for which resonance chains have also been observed, would then need a construction of more and more complicated transfer operators. We will thus choose a different approach and work directly with the zeta functions which turns out to be much more flexible. Looking at equation (12) the choice of the Poincaré section appears only in the order function n_{BS} . This order function has been defined as the length of the prime B -orbit which is associated to the primitive geodesic γ and it is exactly given by the number of times the geodesic passes one of the cut lines in figure 7. Instead of constructing another Poincaré section we can also directly modify the zeta function and we can introduce for each map

$$\mathbf{n} : P_X \rightarrow \mathbb{N}$$

the *generalized zeta function*

$$d_{\mathbf{n}}(s, z) := \prod_{\gamma \in P_X} \prod_{m=0}^{\infty} \left(1 - z^{\mathbf{n}(\gamma)} e^{-(s+m)l(\gamma)} \right). \quad (13)$$

Of course for a general order function \mathbf{n} it is not directly clear where this product converges and whether it has an analytic extension. For all order functions that will appear in the sequel, one can, however, show, that such an analytic extension exists and we refer to [37] for a rigorous proof. The important observation is now that changing the order function only changes the values of the dynamical zeta functions for $z \neq 1$ and the important relation

$$d_{\mathbf{n}}(s, 1) = Z_X(s) \quad (14)$$

is still true. We can therefore define in analogy to the spectrum of the transfer operator (8), the *generalized spectrum*

$$\sigma_s^{(\mathbf{n})} := \{z \in \mathbb{C} \setminus \{0\}, d_{\mathbf{n}}(s, 1/z) = 0\}. \quad (15)$$

From (14) we conclude that also for this generalized spectrum we have the important relation

$$s \in \text{Res}_X \Rightarrow 1 \in \sigma_s^{(\mathbf{n})}.$$

Thus instead of tracing the eigenvalues of a transfer operator we can follow the generalized spectral values while interpolating between different resonances on one chain. The order function which would correspond to a Poincaré section of the symmetric surface $X_{12,12,12}$ with a homogeneous return time counts for each closed geodesic how often it winds around one of the funnels. In figure 9 we traced the generalized spectrum while we interpolate between the same two resonances as in figure 8 and indeed we observe that the generalized spectral value which equals 1 for $s = s_1$ starts to turn around zero and creates all the other resonances on this chains by passing through $z = 1$. Additionally we see in figure 9 that if the s -values follow the path which is suggested by the resonance chains, then the generalized spectral value stays on the unit circle. The continuous lines on which the resonances lie can thus be understood by the real analytic variety

$$\mathcal{C}_{\mathbf{n}} = \{(s, z) \in \mathbb{C}^2, d_{\mathbf{n}}(s, z) = 0, |z| = 1\}. \quad (16)$$

Precisely they are again given by $\text{Pr}_s(\mathcal{C}_{\mathbf{n}})$, the projection of this variety on the s -component.

This approach of working with a generalized zeta function immediately allows us to understand resonance chains for non-symmetric surfaces, as well. These chains have first been observed by Borthwick, for example for the surface $X_{12,13,14}$ (cf. [3, Figure 7]). A homogeneous return time would here require to cut one turn around the first funnel into 12 pieces, one turn around the second funnel into 13 and a turn around the third funnel into 14 pieces. We therefore define for $n_1 = 12, n_2 = 13, n_3 = 14$ the order function

$$\mathbf{n} : \begin{cases} P_X & \rightarrow \mathbb{N} \\ \gamma & \mapsto \sum_{i=1}^3 n_i w_i(\gamma) \end{cases} \quad (17)$$

where $w_i(\gamma)$ counts the windings of the geodesic around the i -th funnel. Figure 10 shows the generalized spectrum for this order function and it perfectly explains the resonance chains. Again the spectral value turns once around the unit circle and creates the next resonance on the chains when the s value moves along the chains. Note that the two other spectral values in $\sigma_{s_1}^{(\mathbf{n})}$ (blue crosses in the left part of figure 10) seem also to lie on the unit circle, which is not the case. Their absolute values are 1.0056 and 1.0032 and they belong to nearby chains, which are visible in the left part

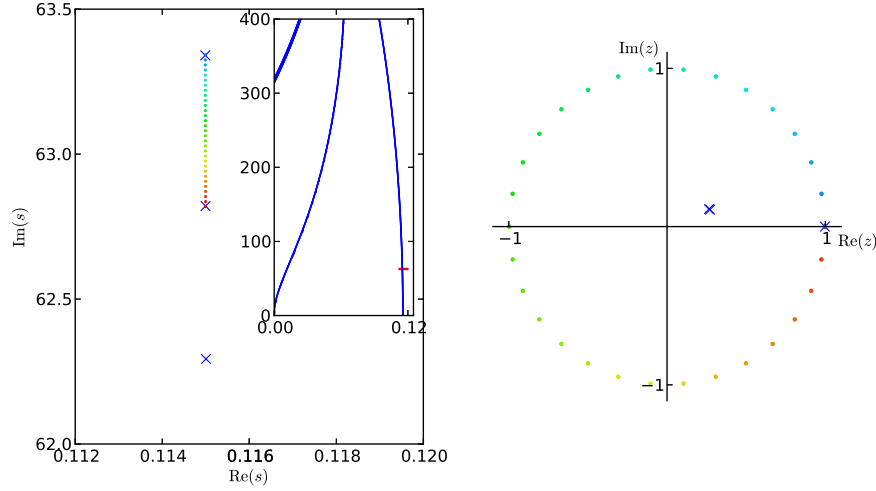


Figure 9. Left: Same as in figure 8. Right: Plot of the generalized spectrum $\sigma_s^{(\mathbf{n})}$ with $|z| > 0.2$ for an order function that counts the number of windings around the funnels. The blue crosses represent the spectrum $\sigma_{s_1}^{(\mathbf{n})}$. By the colored dots we follow the evolution of the spectral value which equals 1 for $s = s_1$. The evolution of the other spectral values is again not plotted.

of figure 10. There are also further spectral values with absolute value slightly smaller than one. We however decided to not plot them in figure 10 for more clarity and as a reliable calculation of the generalized spectrum becomes more and more complicated for small absolute values of z as the order function \mathbf{n} appears with high exponents (cf. Appendix B).

3.3. The length spectrum and existence of resonance chains

From the examples in the previous section we have learned that the resonance chains for symmetric as well as for asymmetric Schottky surfaces are best understood in terms of the generalized zeta function for a suitable choice of an order function. Up to now we have only presented two examples in (figure 9 and figure 10) together with a good choice of an order function but we have not yet clearly worked out under which circumstances it is possible to construct a “good” order function. We will see that this question automatically leads us to a condition on the observability of resonance chains.

The primitive length spectrum, which contains the lengths of all primitive closed geodesics, repeated by multiplicity, can be seen for $X_{12,12,12}$ in figure 11 and for $X_{12,13,14}$ in figure 12. We see that the length spectra of both surfaces form a clear clustering on multiples of a base length ℓ .

The big difference between these two cases is that the common base length to all clusters is $\ell = 12$ for $X_{12,12,12}$ and $\ell = 1$ for $X_{12,13,14}$. Analyzing the two order functions which we have used in these examples, we observe that they exactly respect this clustering: All geodesics of one cluster are mapped to the same integer which is given by the multiple of the base length ℓ on which the cluster is located. All geodesics

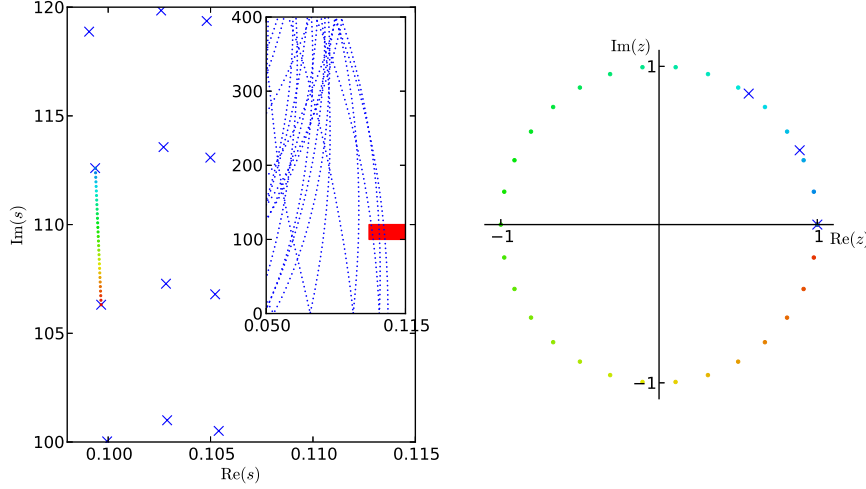


Figure 10. Left: Plot of the resonances of $X_{12,13,14}$. The inset shows the chain structure of the resonances on a large domain in the complex plane. The main plot shows a zoom into one chain, such that the individual resonances become better distinguishable (blue crosses). For orientation the region of the zoom is indicated in the inset by a red rectangle. The colored dots between the two resonances $s_1 = 0.09966 + 106.31i$ and $s_2 = 0.09938 + 112.59i$ represent a discrete interpolation between the two resonances following the line suggested by the resonance chains. Right: generalized spectrum for the order function as defined in (17) with $n_1 = 12, n_2 = 13, n_3 = 14$ for spectral values with $|z| > 0.995$. The blue crosses represent the spectrum $\sigma_{s_1}^{(n)}$. By the colored dots we follow the evolution of one spectral value as the s -values evolve as indicated by the colored points in the right panel. We only follow the evolution of the spectral value starting at 1 for $s = s_1$ for more clarity.

that are necessary to be taken into account for the calculation of the resonances fulfill very well the approximation

$$l(\gamma) \approx \mathbf{n}(\gamma) \cdot \ell. \quad (18)$$

If this condition is exactly fulfilled, then this will lead, similar to the case of a constant return time in Section 2.2, to the existence of straight resonance chains. In fact under this assumption the generalized zeta function could be written as

$$d_{\mathbf{n}}(s, z) := \prod_{\gamma \in P_X} \prod_{m=0}^{\infty} \left(1 - (ze^{-s\ell} e^{-m\ell})^{\mathbf{n}(\gamma)} \right),$$

and if $s_0 \in \text{Res}_X$, i.e. $d_{\mathbf{n}}(s_0, 1) = 0$ then for all $b \in \mathbb{R}$ also $d_{\mathbf{n}}(s_0 + ib, e^{ib\ell}) = 0$. This condition, however, directly implies that $s_0 + 2\pi ki/\ell \in \text{Res}_X$ for each $k \in \mathbb{Z}$, so all resonances would equidistribute on straight lines with a distance of $2\pi/\ell$. Note that for the hyperbolic cylinder (18) is exactly fulfilled and the resonance spectrum is known to be ordered along straight lines [2, Section 5.1]. For non-elementary surfaces (18) can, however, only hold approximately, and one thus expects that these straight chains start to bend and that the spacing of the resonances along the chains becomes more irregular.

We therefore can formulate the following hypothesis:

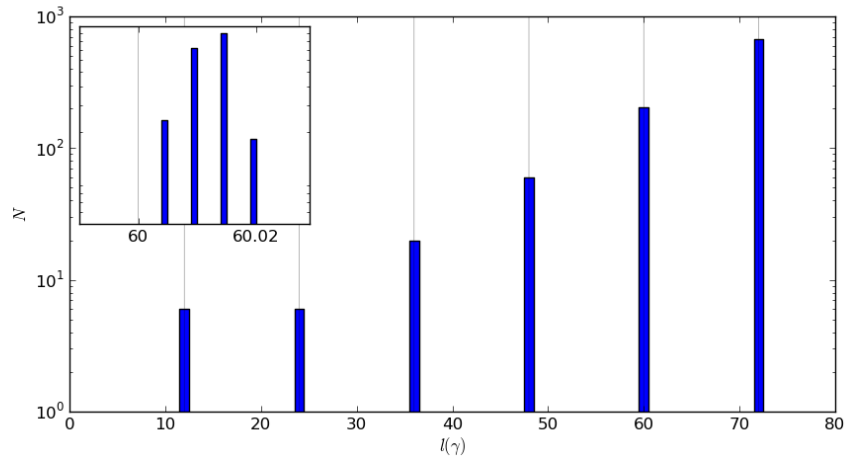


Figure 11. Histogram of the primitive length spectrum for the surface $X_{12,12,12}$. The thin light lines indicate the integer multiples of the base length 12 and one observes that the lengths form clear clusters around these values. This clustering is however not perfect as can be seen in the inset where a histogram with a much smaller binsize resolves the peak at a length around 60.

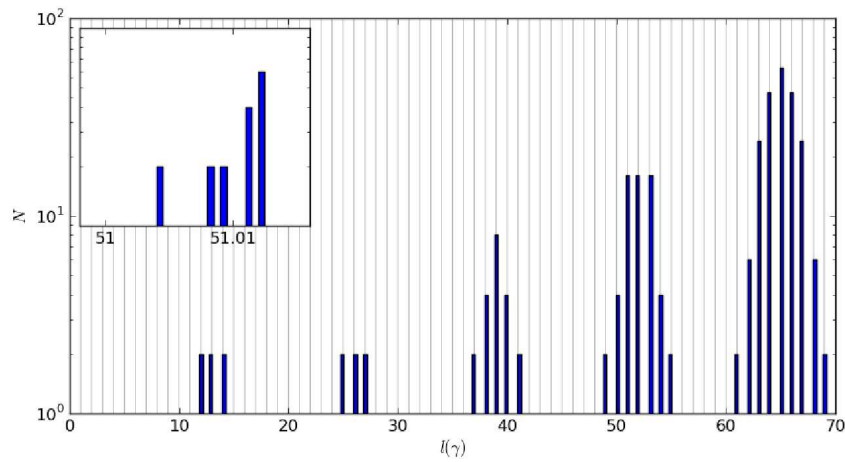


Figure 12. Histogram of the primitive length spectrum for the surface $X_{12,13,14}$. The thin light lines indicate the integer multiples of the base length 1 and one observes that the lengths form clear clusters around these values. Again this clustering is not perfect as can be seen in the inset where a histogram with a much smaller binsize resolves the peak at a length around 51.

If the primitive length spectrum of an infinite volume Riemannian surface (or an open Euclidean billiard) forms clusters at integer multiples of a base length, i.e. if there is a length ℓ and an order function $\mathbf{n} : P_X \rightarrow \mathbb{N}$ such that (18) holds, then one will observe resonance chains. These chains will be described by the projection $\text{Pr}_s(\mathcal{C}_{\mathbf{n}})$ of the analytic variety $\mathcal{C}_{\mathbf{n}} := \{d_{\mathbf{n}} = 0\} \cap \{|z| = 1\}$ to the s -component and the resonances will be approximately spaced by a distance of $2\pi/\ell$ on these lines. The worse the approximation (18) is fulfilled, the stronger the chains will bend and the more irregular the resonance distribution on the chains will become.

Of course (18) cannot hold on the whole length spectrum, but recall that for the calculation of the resonances in a bounded subset of a complex plane, one only needs finitely many geodesics. We thus suppose that the chains will be observable in this bounded domain, if (18) is fulfilled on the geodesics which are necessary for their calculation.

4. Further tests of the Hypothesis

We already saw several examples in Section 2.2 and 3.2 which support our hypothesis on the existence of resonance chains. We will now test its validity against some more examples. First of all our condition should be able to explain the non-observability of resonance chains in some systems which are structurally similar to systems which show resonance chains.

For example one observes that symmetric 3-disk billiards only show resonance chains if the disks are sufficiently far away from each other. The resonance spectrum of the symmetric 3-disk billiard with $R/a = 3$ shows no chain structure contrary to the more open case with $R/a = 6$ (see figure 13). This is easily understood by looking at the primitive length spectrum. While for $R/a = 6$ one sees a clear clustering of the lengths, the length spectrum for $R/a = 3$ equidistributes very quickly and it is impossible to choose an order function which fulfills (18). Our hypothesis also explains why symmetric 4-disk systems show in general no chain structure (see e.g. FIG. 13 in [10] for the Ruelle resonances of a 4-disk system) whereas the 3-dimensional 4-sphere billiard shows them: If 4 disks are distributed on a square, the lengths between two neighboring disks and the length between diagonal disks are in general not multiples of each others but form two incommensurable base lengths, so it will not be possible to construct a good order function. For the 4-sphere billiard where the spheres are placed on a regular tetrahedron, the distance between an arbitrary pair of spheres is equal and, if the spheres are sufficiently far away from each other, one expects a clustering of the length spectrum on multiples of this base length. Exactly in this case of sufficiently open 4-sphere billiards the chain structure has been observed (cf. Figure 5.2-5.9 in [5]).

We will end this section by using the predictive power of our hypothesis in order to identify a new interesting system which shows the coexistence of two chains. As we only demand (18) to hold approximately there should be examples for which there are different compatible base lengths and order functions, e.g. the surface $X_{12,12,13}$. As can be seen in figure 14 the length spectrum can be either interpreted as forming clusters at multiples of the base length $\ell = 12$ or at multiples of the base length $\ell = 1$. The hypothesis thus predicts two different chain structures, one where the resonances are spaced by a distance of $2\pi/12$ and another one with a larger spacing of 2π . As for $\ell = 12$ the approximation (18) holds much worse then for $\ell = 1$ our hypothesis predicts that the resonance chains belonging to $\ell = 12$ are much more twisted then the chains

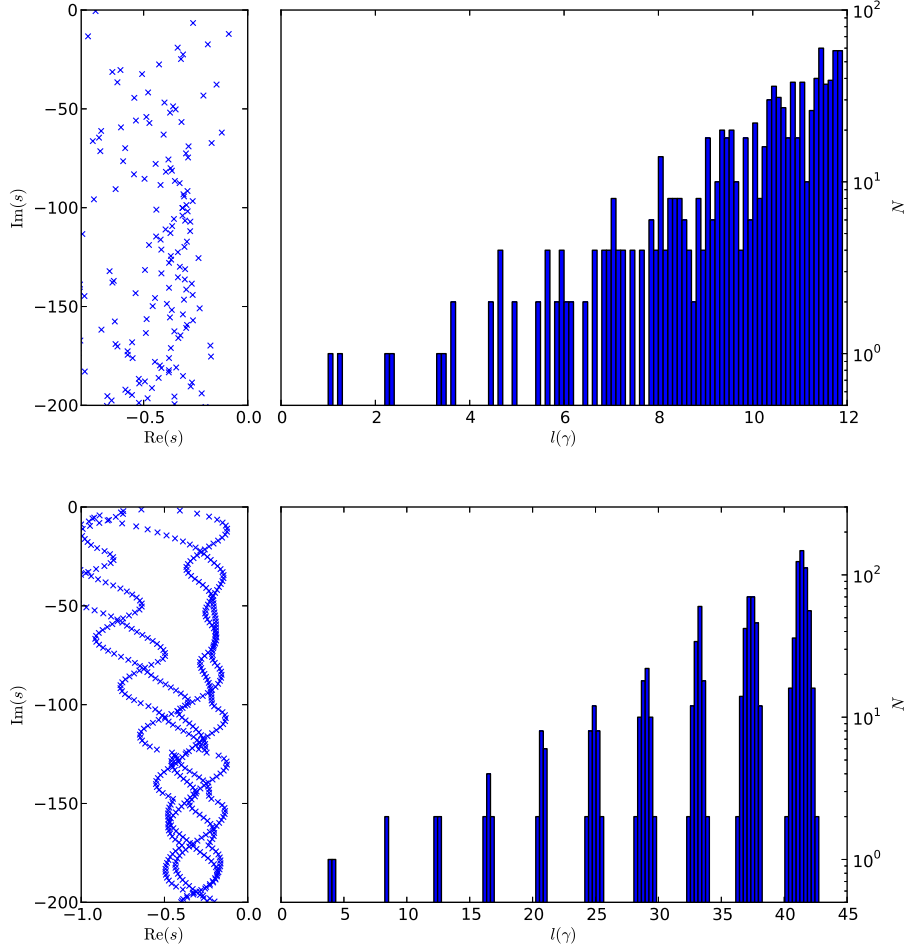


Figure 13. Comparison of the resonance structure (left) with the primitive length spectrum (right) of the symmetry reduced 3-disk system for $R/a = 3$ (upper plot) and $R/a = 6$ (lower plot). While for $R/a = 6$ one observes a clear clustering of the lengths and an obvious chain structure in the resonances, the lengths equidistribute very quickly and there are no visible chains in the resonance spectrum.

belonging to $\ell = 1$. As figures 15 and 16 show, all these predictions are observed in the resonance structure. Choosing the order function (17) with $n_1 = n_2 = n_3 = 1$ which corresponds to the base length $\ell = 12$ we observe strongly twisted resonance chains as indicated by the red circles in the left part of figure 15. The generalized spectrum $\sigma_s^{(\mathbf{n})}$ of this order function creates this kind of chains by the rotating spectral values and if one connects neighboring resonances on this chain by the continuous line which is suggested by the chain structure, the generalized spectral value moves along the unit circle. This verifies that the chains are described by $\text{Pr}_s(\mathcal{C}_{\mathbf{n}})$. Choosing, however, the order function (17) with $n_1 = n_2 = 12, n_3 = 13$ which is the corresponding choice for the base length $\ell = 1$ we obtain a generalized zeta function which describes a second

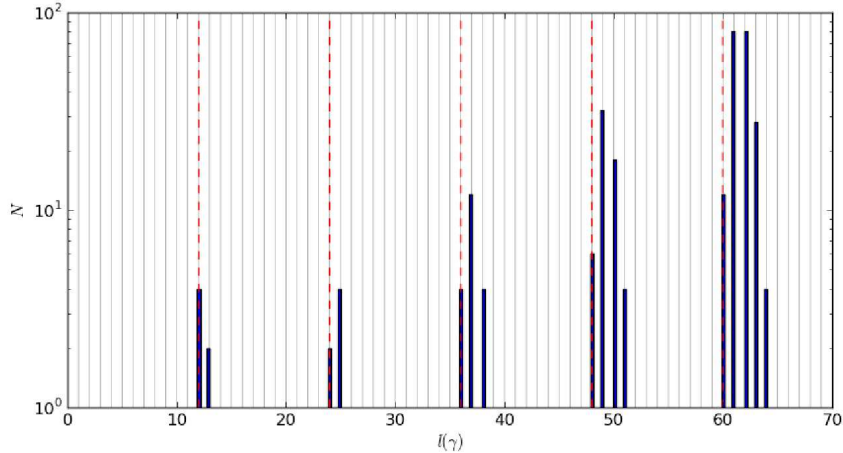


Figure 14. Histogram of the primitive length spectrum for the Schottky surface $X_{12,12,13}$. The thin light lines indicate the integer multiples of the base length $\ell = 1$ and red dashed lines the multiples of a second base length $\ell = 12$. One can observe two types of clustering, one very coarse clustering around the multiples of $\ell = 12$ and a much finer clustering around the multiples of $\ell = 1$.

structure of resonance chains, on which the resonance distances are much larger and which are much straighter (see figure 16).

5. Conclusion

In this article we presented a unifying approach to the chain structure of quantum resonances, classical Ruelle resonances and geometric resonances. We showed at the example of 3-disk systems and Schottky surfaces that the resonance chains can be understood in all three cases by means of a generalized zeta function $d_{\mathbf{n}}(s, z)$ which depends on the choice of an order function $\mathbf{n} : P \rightarrow \mathbb{N}$ on the set of primitive closed classical orbits P . The central property of this generalized zeta function is that independent of the choice of the order function the resonances are given by the zeros of zeta function $Z(s) = d_{\mathbf{n}}(s, 1)$. We showed that if the order function is chosen such that

$$l(\gamma) \approx \mathbf{n}(\gamma)\ell \quad (19)$$

for an arbitrary base length ℓ then the second complex variable allows to interpolate between the resonances of one chain. Furthermore we demonstrated that the continuous lines where the resonances are found on are given by the projection onto the s -component of the real analytic variety

$$\mathcal{C}_{\mathbf{n}} = \{d_{\mathbf{n}}(s, z) = 0\} \cap \{|z| = 1\}.$$

The existence of an order function that fulfills the condition (19) does of course depend on the structure of the length spectrum of the classical system. This led us to the hypothesis that the existence of resonance chains is directly linked to a clustering of the classical length spectrum that allows us to choose an order function according to (19). We finally validated this hypothesis by presenting several examples of systems

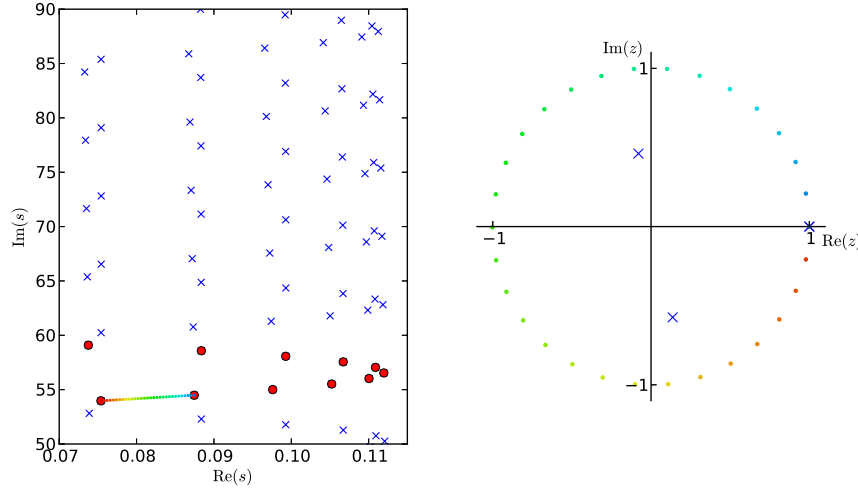


Figure 15. Left: The resonances of $X_{12,12,13}$ in the complex plane are marked by crosses. The red circles highlight the resonances on the chain, which belongs to the base length $\ell = 12$. The colored dots between the two resonances $s_1 = 0.07539 + 53.97i$ and $s_2 = 0.08746 + 54.49i$ represent a discrete interpolation between the two resonances following the line suggested by the resonance chains. Right: generalized spectrum for the order function as defined in (17) with $n_1 = n_2 = n_3 = 1$. The blue crosses represent the spectrum $\sigma_{s_1}^{(n)}$ for $|z| > 0.2$. By the colored dots we follow the evolution of the spectral value which equals one while interpolating the s -values between s_1 and s_2 as indicated by the colored points on the left.

with and without resonance chains. In all cases the resonance chains were found to be linked to a clustering of the length spectrum. Furthermore we showed that this new understanding allows to construct scattering systems with a customized resonance chain structure. This control of the resonance chains could be of importance in microdisk cavities where similar resonance chains have already been observed [39] and where a precise control of the resonance position in the complex plane is of great interest for their application as microdisk lasers.

Additionally this understanding is crucial for fundamental questions in quantum chaos. In chaotic systems the clear clusters in the length spectrum will only exist for short lengths. For larger lengths the clusters become broader and broader and will finally overlap. However, we required the condition (19) only to hold in the length range which is necessary for the calculation of the resonances in the studied frequency regime. In other words for the existence of resonance chains in a given frequency range, condition (19) only has to hold for the lengths which can be resolved by the Planck cells at this frequency. If one still observes resonance chains, then one has to keep in mind that one is not yet at high enough frequencies to resolve the length spectrum in a regime, where the clusters dissolve. This could be especially important for the test of results that are obtained by arguing with phase cancellation such as the conjectures on the improved spectral gaps [17]

Finally the study of resonance chains opens a variety of mathematical questions. We numerically observed in this article that the chain structure becomes the clearer

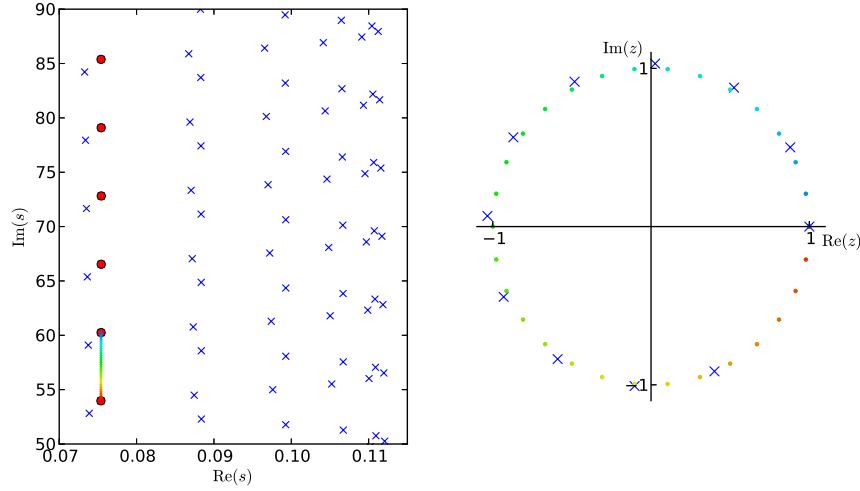


Figure 16. Left: The resonances of $X_{12,12,13}$ in the complex plane are marked by crosses. The red circle highlight the resonances on the chain, which belongs to the base length $\ell = 1$. The colored dots between the two resonances $s_1 = 0.07539 + 53.97i$ and $s_2 = 0.07542 + 60.25i$ represent a discrete interpolation between the two resonances following the line suggested by the resonance chains. Right: generalized spectrum for the order function as defined in (17) with $n_1 = n_2 = n_3 = 1$. The blue crosses represent the spectrum $\sigma_{s_1}^{(n)}$ for $|z| > 0.99$. By the colored dots we follow the evolution of the spectral value which equals one while interpolating the s -values between s_1 and s_2 as indicated by the colored points on the left.

the better condition (19) is fulfilled. By studying not just a single system but a whole family of scattering systems, where (19) is increasingly well fulfilled in a certain limit one can then try to prove the existence of resonance chains asymptotically in this limit. Furthermore one can try to give precise, simple formulas for the location of these chains. For symmetric 3-disk systems this limit would correspond to large R/a -values and for Schottky surfaces to large funnel widths. For the latter case, first results into this direction will be presented in [37].

Acknowledgments

We are grateful to Ulrich Kuhl for many interesting stimulating discussions and detailed feedback concerning this work. Furthermore we thank Bruno Eckhardt, David Borthwick, Stéphane Nonnenmacher, Pablo Ramacher and Gabriel Rivière for discussions and comments. This work was supported by the project ANR 2009-12 METHCHAOS. S.B. acknowledges financial support by DFG via the project FOR760 and T.W. by the German National Academic Foundation.

Appendix A. Derivation of the product form for dynamical zeta function

In this appendix we will recall the derivation of the product form (5) from the definition of the dynamical zeta function as it has been defined in (4) by the flat trace

$$d^b(z) := \exp \left(- \sum_{n>0} \frac{z^n}{n} \sum_{x \in \text{Fix}(\phi^n)} \frac{V_n(x)}{|\det(1 - (D\phi^n)(x))|} \right).$$

For each fixed point $\phi^n(x) = x$ the Jacobian is a hyperbolic, symplectic 2×2 matrix and it thus has two real eigenvalues Λ_n and $1/\Lambda_n$ with $|\Lambda_n| > 1$ and the determinant can be written as

$$\begin{aligned} \frac{1}{|\det(1 - (D\phi^n)(x))|} &= \frac{1}{|1 - \Lambda_n||1 - 1/\Lambda_n|} \\ &= |\Lambda_n|^{-1} \left(\sum_{r \geq 0} \Lambda_n^{-r} \right) \left(\sum_{s \geq 0} \Lambda_n^{-s} \right) \\ &= |\Lambda_n|^{-1} \sum_{k \geq 0} (k+1) \Lambda_n^{-k} \end{aligned} \quad (\text{A.1})$$

where for the last equality we used that a positive integer k can be written as $k+1$ different sums of two positive integers r and s .

As a next step we can treat the double sum $\sum_{n>0} \sum_{x \in \text{Fix}(\phi^n)}$ which is simply the sum over all fixed points of ϕ^n for arbitrary length ϕ . First we note that the iterated product of the potential function $V_n(x)$ as well as the instable eigenvalue Λ_n do not depend on the choice of the fixed point in a fixed orbit $\{x, \phi(x), \dots, \phi^{n-1}(x)\}$. Additionally we see that if an orbit of length $m \cdot n_p$ is a m -times iterate of a primitive orbit of length n_p , then the orbit contains n_p fixed points and as well the iterated product as the instable eigenvalue are the m -th power of the values from the primitive orbit

$$V_{m \cdot n_p}(x) = (V_{n_p}(x))^m \text{ and } \Lambda_{m \cdot n_p} = \Lambda_{n_p}^m.$$

This allows us to write the double sum $\sum_{n>0} \sum_{x \in \text{Fix}(\phi^n)}$ as a double sum over all primitive periodic orbits and their repetitions $\sum_{p \in P} \sum_{m>0}$ and we obtain

$$\begin{aligned} d^b(z) &= \exp \left(- \sum_{k \geq 0} (k+1) \sum_{n>0} \sum_{x \in \text{Fix}(\phi^n)} \frac{z^n}{n} V_n(x) |\Lambda_n|^{-1} \Lambda_n^{-k} \right) \\ &= \exp \left(- \sum_{k \geq 0} (k+1) \sum_{p \in P} \sum_{m>0} \frac{z^{n_p \cdot m}}{m} (V_{n_p}(x))^m \left(|\Lambda_{n_p}| \Lambda_{n_p}^{-k} \right)^m \right) \\ &= \prod_{k \geq 0} \prod_{p \in P} \left[\exp \left(- \sum_{m>0} \frac{\left(z^{n_p} V_{n_p}(x) |\Lambda_{n_p}|^{-1} \Lambda_{n_p}^{-k} \right)^m}{m} \right) \right]^{k+1} \\ &= \prod_{k \geq 0} \prod_{p \in P} \left[1 - z^{n_p} \frac{V_{n_p}(x)}{|\Lambda_{n_p}| \Lambda_{n_p}^k} \right]^{k+1} \end{aligned}$$

where we used the Taylor series of $\log(1-x)$ in the last equality.

Appendix B. Numerical considerations for the calculation of the generalized spectrum $\sigma_s^{(\mathbf{n})}$

In this appendix we will shortly recall how the resonance spectrum on Schottky surfaces is usually calculated (see [18, 14, 3] for more details) and what modifications have to be performed for the calculation of the generalized zeta function and the generalized spectrum.

Usually the resonance spectrum is obtained by Taylor expanding (11) in z around zero

$$d_{BS}(s, z) = \sum_{k=0}^{\infty} z^k b_k(s).$$

The Taylor coefficients are then explicitly given by [18, Proposition 8]

$$b_k(s) = \sum_{r=1}^k \sum_{(n_1, \dots, n_r) \in P(k, r)} \frac{(-1)^r}{r!} \prod_{l=1}^r \frac{1}{n_l} \sum_{u \in \text{Fix}(B^{n_l})} \frac{((B^{n_l})'(u))^{-s}}{1 - (B^{-n_l})'(u)} \quad (\text{B.1})$$

where $P(k, r)$ are all r -partitions of k , i.e. all r -tuples of integers whose sum equals k . The numerical task in order to calculate these coefficients then consists in calculating the stabilities $(B^n)'(u)$ of sufficiently many fixed points. For a 3-funneled Schottky surface X_{l_1, l_2, l_3} this can efficiently be done using the generators of the corresponding Schottky group and a symbolic dynamic. For X_{l_1, l_2, l_3} the generators can be written as

$$S_1 = \begin{pmatrix} \cosh(l_1/2) & \sinh(l_1/2) \\ \sinh(l_1/2) & \cosh(l_1/2) \end{pmatrix}, \quad S_2 = \begin{pmatrix} \cosh(l_2/2) & a \sinh(l_2/2) \\ a^{-1} \sinh(l_2/2) & \cosh(l_2/2) \end{pmatrix},$$

where the parameter a is chosen such that $\text{Tr}(S_1 S_2^{-1}) = -2 \cosh(l_3/2)$ and as usual one writes $S_3 = S_1^{-1}$ and $S_4 = S_2^{-1}$. If we then define the set of words of length n by

$$\mathcal{W}_n := \left\{ w \in \{1, 2, 3, 4\}^n, |w_{j+1} - w_j| \neq r \text{ for } j = 1, \dots, n-1 \text{ and } |w_1 - w_n| \neq r \right\}$$

then we can define for each $w \in \mathcal{W}_n$ the hyperbolic isometry

$$S_w := S_{w_1} S_{w_2} \dots S_{w_n}.$$

One then can easily show from the definition of the Bowen-Series maps [2, Section 15.2] that for each $u \in \text{Fix}(B^n)$ there is exactly one $w \in \mathcal{W}_n$ and

$$\Lambda(w) := 2 \cosh^{-1} \left(\frac{|\text{Tr}(S_w)|}{2} \right) = (B^n)'(u)$$

which allows an efficient calculation of (B.1) and thus of $d_{BS}(s, z)$.

For the calculation of $d_{\mathbf{n}}(s, z)$ one analogously has to Taylor-expand the zeta function in z around zero

$$d_{\mathbf{n}}(s, z) = \sum_{k=0}^{\infty} z^k b_k^{(\mathbf{n})}(s).$$

Then one has to calculate the new Taylor coefficients $b_k^{(\mathbf{n})}(s)$. As we want to use the word coding to calculate the lengths of the geodesics or the stabilities $(B^n)'(u)$, respectively, we first have to transfer the order function $\mathbf{n} : P_{X_{l_1, l_2, l_3}} \rightarrow \mathbb{N}$ to an order function on $\mathcal{W} = \bigcup_{n>0} \mathcal{W}_n$. This transformation can be obtained via the correspondence between closed geodesics on X_{l_1, l_2, l_3} and fixed points of B [2,

Proposition 15.5]. Using this identification one calculates that the order function as defined in (17) is then given by

$$\mathbf{n}(w) = n(w_1, w_2) + n(w_2, w_3) + \dots + n(w_n, w_1) \quad (\text{B.2})$$

where

$$\begin{aligned} n(1, 1) &= n(3, 3) = n_1, & n(2, 2) &= n(4, 4) = n_1 \\ n(1, 4) &= n(4, 1) = n(2, 3) = n(3, 2) = n_3/2 \\ n(1, 2) &= n(2, 1) = n(3, 4) = n(4, 3) = (n_1 + n_2)/2. \end{aligned}$$

The Bowen-Series order function \mathbf{n}_{BS} can be translated much more easily. From its definition in Section 3.1 it immediately follows, that $\mathbf{n}_{BS}(w) = n$ for all $w \in \mathcal{W}_n$.

Using the order function on the words as well as the identification of fixed points and words, equation (11) can be written as

$$d_{BS}(s, z) = \exp \left(- \sum_{j>0} \frac{1}{j} \sum_{w \in \mathcal{W}_j} z^{\mathbf{n}_{BS}(w)} \frac{\Lambda(w)^{-s}}{1 - \Lambda(w)^{-1}} \right).$$

Starting with (13) and reversing the argumentation of Appendix A the generalized zeta function $d_{\mathbf{n}}(s, z)$ can be written as

$$d_{\mathbf{n}}(s, z) = \exp \left(- \sum_{j>0} \frac{1}{j} \sum_{w \in \mathcal{W}_j} z^{\mathbf{n}(w)} \frac{\Lambda(w)^{-s}}{1 - \Lambda(w)^{-1}} \right). \quad (\text{B.3})$$

An analogous calculation to those in [18, Proposition 8] then gives us the formula for the Taylor coefficients

$$b_k^{(\mathbf{n})}(s) = \sum_{r=1}^k \sum_{(n_1, \dots, n_r) \in P(k, r)} \frac{(-1)^r}{r!} \prod_{l=1}^r \sum_{j>0} \frac{1}{j} \sum_{w \in \mathcal{W}_j, \text{s.t. } \mathbf{n}(w)=n_l} \frac{\Lambda(w)^{-s}}{1 - \Lambda(w)^{-1}}. \quad (\text{B.4})$$

The stabilities $\Lambda(w)$ can be calculated by the generators S_i of the Schottky group as described above and in order to simplify the combinatorial task of building together the Taylor coefficients $b_k^{(\mathbf{n})}(s)$ from these stabilities we can use the same recurrence trick as presented in [14]. We therefore write

$$B_{k,r}^{(\mathbf{n})}(s) := \sum_{(n_1, \dots, n_r) \in P(k, r)} \frac{(-1)^r}{r!} \prod_{l=1}^r a_{n_l}^{(\mathbf{n})}(s)$$

and

$$a_n^{(\mathbf{n})}(s) := \sum_{j>0} \frac{1}{j} \sum_{w \in \mathcal{W}_j, \text{s.t. } \mathbf{n}(w)=n} \frac{\Lambda(w)^{-s}}{1 - \Lambda(w)^{-1}}.$$

We can then use the recurrence relations

$$B_{k,r}^{(\mathbf{n})} = \frac{1}{r} \sum_{l=1}^{k-r+1} B_{k-l, r-1}^{(\mathbf{n})}(s) a_l^{(\mathbf{n})}(s).$$

The only difference in calculating the generalized zeta function compared to the dynamical zeta function of the Bowen-Series maps thus consists in the modified formula for the functions $a_n^{(\mathbf{n})}(s)$.

Note that as $d_{\mathbf{n}}(s, z)$ is analytic the Taylor coefficients $b_k^{(\mathbf{n})}(s)$ decay superexponentially in k and theoretically one can compute $d_{\mathbf{n}}(s, z)$ for arbitrary (s, z) .

Practically, however, the convergence becomes worse and worse the smaller $\text{Re}(s)$ and the bigger $|z|$ become. Especially for order functions (17) with larger values of n_1, n_2, n_3 as they appeared for example for the surfaces $X_{12,13,14}$ the convergence depends very strongly on $|z|$. This implies that a reliable calculation of $d_{\mathbf{n}}$ is only possible for z values which are slightly greater than 1. In terms of the generalized spectrum this implies that the numerical calculation is only possible for z slightly smaller than 1. As the interesting region for the understanding of the resonance chains is, however, the unit circle, this is no severe problem for the numerical investigations presented in this article.

Appendix C. Topological pressure and analyticity of $d^{(b)}(s, z)$

The topological pressure of a 3-disk system is a function $P(\beta)$ of a positive parameter $\beta > 0$ that describes the convergence behavior of certain zeta functions. Writing

$$V_s^\beta(x) := |\Lambda(x)|^{1-\beta} e^{-s\tau(x)}$$

the topological pressure of the 3-disk system can be defined [12] to be the real number $P(\beta)$ such that

$$d_\beta(s) := \det(1 - \mathcal{L}_{V_s^\beta}) = \exp \left(- \sum_{n>0} \frac{1}{n} \sum_{x \in \text{Fix}(\phi^n)} \frac{(V_s^\beta)_n(x)}{|\det(1 - (D\phi^n)(x))|} \right)$$

is absolutely convergent for $\text{Re}(s) > P(\beta)$. This directly implies that $d^{(a)}$ has no zeros for $\text{Re}(s) > P(1/2)$ and that $d^{(b)}(s)$ has no zeros for $\text{Re}(s) > P(3/2)$. For a symmetric 3-disk system with $R/a = 6$ this value of the topological pressure is given by

$$P(3/2) = -0.699.$$

Consequently all zeros of the Gutzwiller-Voros zeta function $Z_{GV}(s, 1)$ with $\text{Re}(s) > -0.699$ are automatically zeros of the Fredholm determinant $d_{(a)}(s, 1)$ and can thus be interpreted by the spectrum of the transfer operator $\mathcal{L}_{V_s^{(a)}}$. Note that all the numerical investigations presented in this article are within this s -range.

- [1] S. Barkhofen, T. Weich, A. Potzweit, H.-J. Stöckmann, U. Kuhl, and M. Zworski. Experimental Observation of the Spectral Gap in Microwave n -Disk Systems. *Phys. Rev. Lett.*, 110:164102, 2013.
- [2] D. Borthwick. *Spectral theory of infinite-area hyperbolic surfaces*. Springer, 2007.
- [3] D. Borthwick. Distribution of resonances for hyperbolic surfaces. *Exp. Math.*, 23:25–45, 2014.
- [4] P. Cvitanović and B. Eckhardt. Periodic-orbit quantization of chaotic systems. *Phys. Rev. Lett.*, 63:823, 1989.
- [5] A. Eberspächer. Fractal Weyl law for three-dimensional chaotic hard-sphere scattering systems. *Diplomarbeit Universität Stuttgart*, 2010.
- [6] A. Eberspächer, J. Main, and G. Wunner. Fractal Weyl law for three-dimensional chaotic hard-sphere scattering systems. *Phys. Rev. E*, 82:046201, 2010.
- [7] F. Faure and N. Roy. Ruelle–Pollicott resonances for real analytic hyperbolic maps. *Nonlinearity*, 19(6):1233, 2006.
- [8] F. Faure and M. Tsujii. Prequantum transfer operator for symplectic Anosov diffeomorphism. *arXiv preprint arXiv:1206.0282*, 2012.
- [9] F. Faure and M. Tsujii. The semiclassical zeta function for geodesic flows on negatively curved manifolds. *arXiv preprint arXiv:1311.4932*, 2013.
- [10] P. Gaspard and D. Alonso Ramirez. Ruelle classical resonances and dynamical chaos: The three- and four-disk scatterers. *Phys. Rev. A*, 45:8383, Jun 1992.
- [11] P. Gaspard and S. A. Rice. Exact quantization of the scattering from a classically chaotic repeller. *J. Chem. Phys.*, 90:2255, 1989.
- [12] P. Gaspard and S. A. Rice. Scattering from a classically chaotic repeller. *J. Chem. Phys.*, 90:2225, 1989.

- [13] P. Gaspard and S. A. Rice. Semiclassical quantization of the scattering from a classically chaotic repeller. *J. Chem. Phys.*, 90:2242, 1989.
- [14] L. Guillopé, K. K. Lin, and M. Zworski. The Selberg Zeta Function for Convex Co-Compact Schottky Groups. *Commun. Math. Phys.*, 245:149, 2004.
- [15] L. Guillopé and M. Zworski. Scattering asymptotics for Riemann surfaces. *The Annals of Mathematics*, 145(3):597–660, 1997.
- [16] M. Ikawa. Decay of solutions of the wave equation in the exterior of several convex bodies. *Ann. Inst. Fourier*, 38:113, 1988.
- [17] D. Jakobson and F. Naud. On the critical line of convex co-compact hyperbolic surfaces. *Geometric and Functional Analysis*, 22(2):352–368, 2012.
- [18] O. Jenkinson and M. Pollicott. Calculating Hausdorff dimension of Julia sets and Kleinian limit sets. *American Journal of Mathematics*, 124(3):495–545, 2002.
- [19] W. Lu, M. Rose, K. Pance, and S. Sridhar. Quantum resonances and decay of a chaotic fractal repeller observed using microwaves. *Phys. Rev. Lett.*, 82:5233, 1999.
- [20] W. T. Lu, S. Sridhar, and M. Zworski. Fractal Weyl Laws for Chaotic Open Systems. *Phys. Rev. Lett.*, 91:154101, 2003.
- [21] R. Mazzeo and R. Melrose. Meromorphic extension of the resolvent on complete spaces with asymptotically constant negative curvature. *Journal of Functional analysis*, 75(2):260–310, 1987.
- [22] S. Nonnenmacher. Spectral problems in open quantum chaos. *Nonlinearity*, 24(12):R123, 2011.
- [23] S. Nonnenmacher, J. Sjöstrand, and M. Zworski. Fractal weyl law for open quantum chaotic maps. *Annals of Math.*, 179(1):179–251, 2014.
- [24] S. Nonnenmacher and M. Zworski. Distribution of resonances for open quantum maps. *Commun. Math. Phys.*, 269(2):311–365, 2007.
- [25] S. Nonnenmacher and M. Zworski. Quantum decay rates in chaotic scattering. *Acta Mathematica*, 203:149, 2009.
- [26] S. Patterson and P. Perry. The divisor of Selberg’s zeta function for Kleinian groups. Appendix A by Charles Epstein. *Duke Math. J.*, 106(2):321–390, 2001.
- [27] V. Petkov and L. Stoyanov. Analytic continuation of the resolvent of the Laplacian and the dynamical zeta function. *Anal. PDE*, 3:427, 2010.
- [28] A. Potzuweit, T. Weich, S. Barkhofen, U. Kuhl, H.-J. Stöckmann, and M. Zworski. Weyl asymptotics: From closed to open systems. *Phys. Rev. E*, 86:066205, 2012.
- [29] D. Ruelle. Zeta-functions for expanding maps and Anosov flows. *Inventiones mathematicae*, 34(3):231–242, 1976.
- [30] H.H. Rugh. The correlation spectrum for hyperbolic analytic maps. *Nonlinearity*, 5(6):1237, 1992.
- [31] H. Schanze. Realisierung von nichteuklidischen Billiards durch Wellenwannen. *Diplomarbeit Universität Marburg*.
- [32] H. Schomerus and J. Tworzydło. Quantum-to-Classical Crossover of Quasibound States in Open Quantum Systems. *Phys. Rev. Lett.*, 93:154102, 2004.
- [33] J. Sjöstrand. Geometric bounds on the density of resonances for semiclassical problems. *Duke Math. J.*, 60:1, 1990.
- [34] H.-J. Stöckmann. *Quantum chaos: an introduction*. Cambridge University Press, 2007.
- [35] B.R. Vainberg. On the analytical properties of the resolvent for a certain class of operator-pencils. *Sbornik: Mathematics*, 6(2):241–273, 1968.
- [36] A. Voros. Unstable periodic orbits and semiclassical quantisation. *J. Phys. A*, 21(3):685, 1988.
- [37] T. Weich. Resonance chains and geometric limits on Schottky surfaces, 2014. *arXiv preprint arXiv:1403.7419*, 2014.
- [38] T. Weich, S. Barkhofen, U. Kuhl, C. Poli, and H. Schomerus. Formation and interaction of resonance chains in the open 3-disk system. *New J. Phys.*, (16):033029, 2014.
- [39] J. Wiersig and J. Main. Fractal Weyl law for chaotic microcavities: Fresnel’s laws imply multifractal scattering. *Phys. Rev. E*, 77:036205, 2008.
- [40] A. Wirzba. Quantum mechanics and semiclassics of hyperbolic n -disk scattering systems. *Phys. Rep.*, 309:1, 1999.
- [41] M. Zworski. Resonances in physics and geometry. *Notices of the AMS*, 46(3):319–328, 1999.